Summer 7-17-2023

The Relationship Between Water Temperature and Proximity to Surface Urban Heat Islands within the Lower Chesapeake Bay Watershed for the Summer of 2019

Sarah Kerner

MSGA Capstone:

The Relationship Between Water Temperature and Proximity to Surface Urban Heat Islands within the Lower Chesapeake Bay Watershed for the Summer of 2019

By

Sarah Kerner

A Capstone Project presented in Fulfillment

of the Requirements for the degree of

Masters in Geospatial Analysis

MSGA Program

University of Mary Washington

Fredericksburg, VA 22401

17 July 2023

Capstone Advisor: Dr. Marco Millones Mayer

Capstone Committee Member: Dr. Jackie Gallagher

Capstone Committee Member: Dr. Scott Allen

Capstone Committee Member: Dr. Elsa Nickl

Abstract

Surface urban heat islands (SUHIs) are land surfaces with high concentrations of impervious surfaces like roofs, roads, sidewalks and other infrastructures that trap, absorb, and re-emit heat throughout the day/night and typically present higher temperatures than their surrounding rural areas. In this study, I evaluate how presence of and distance to SUHIs are associated with water temperature in the lower Chesapeake Bay watershed for the summer of 2019. When heavy precipitation events occur, flooding creates stormwater runoff, which is exposed to the hotter temperatures in urban areas. This introduces thermal pollution to nearby rivers and streams disrupting aquatic ecosystems. The hypothesis for this research is that the closer water temperature points are to SUHIs, the warmer the temperature measured will be. To assess this, I processed Landsat 8 and 9 scenes in order to derive land surface temperature (LST), normalized difference vegetation index (NDVI), and normalized difference build-up index (NDBI). I also processed land cover from the national land cover dataset (NLCD) and a digital elevation model (DEM) from which I derived flow direction (FD) and flow accumulation (FA). I used water temperatures measured by water quality stations from 25 sources as well. If areas with a surface temperature were half a standard deviation above the agricultural land cover LST average, they were defined as SUHIs, following Kaplan et al. (2018). The other datasets were used to extract other factors that can impact temperature or the relationship between distance to SUHIs and temperature. In addition, I also processed local climate zones (LCZs) to validate the identified SUHIs. To extract distance from SUHI areas and the water temperature datapoints, I used ArcGIS's Euclidean Distance and Direction Distance tools. These were calculated for various cases, including; no-distance (contained within SUHI), omni-directional distance, and upstream/downstream distance. Some of these methodological attempts were more successful

than others. Overall results do not show a strong relationship between warmer water temperatures and proximity to SUHIs; therefore, in general terms, the hypothesis is not supported. However, there are some noteworthy findings; a) there are warmer water temperatures near urban centers where most of the SUHIs are located; b) elevation has the strongest influence and highest significance on water temperature with the trends of the variables explored (i.e., at higher elevations, the water temperature is cooler while at lower elevations, the water temperature is warmer); and, c) Euclidean distance to SUHIs and NDVI are other significant factors. With more time and resources, I would include more data on environmental confounding factors and use improved methods to calculate various distance measures, which would likely help tease out more specific relationships between water temperature and SUHIs as well as to interpret their correlations.

Table of Contents

List of Figures

List of Tables

1. Introduction and Background

Urban structures, such as asphalt roads and buildings, absorb and re-emit the heat from the sun more than the forests and agricultural areas nearby. Cities, where the urban infrastructures are highly concentrated and vegetation land covers are limited, become heat islands. Macarof and Statescu (2017) define urban heat islands (UHIs) as "the phenomenon of higher atmospheric and surface temperatures occurring in the urban area or metropolitan area than in the surrounding rural areas due to urbanization." Figure 1 illustrates the fluctuating temperature for the different land covers below. Weather and geography also play a role in the influence of temperatures. For example, "calm and clear weather conditions result in more severe heat islands by maximizing the amount of solar energy reaching urban surfaces and minimizing the amount of heat that can be carried away," and "nearby mountains can block wind from reaching a city or create wind patterns that pass through a city" (EPA 2022c).

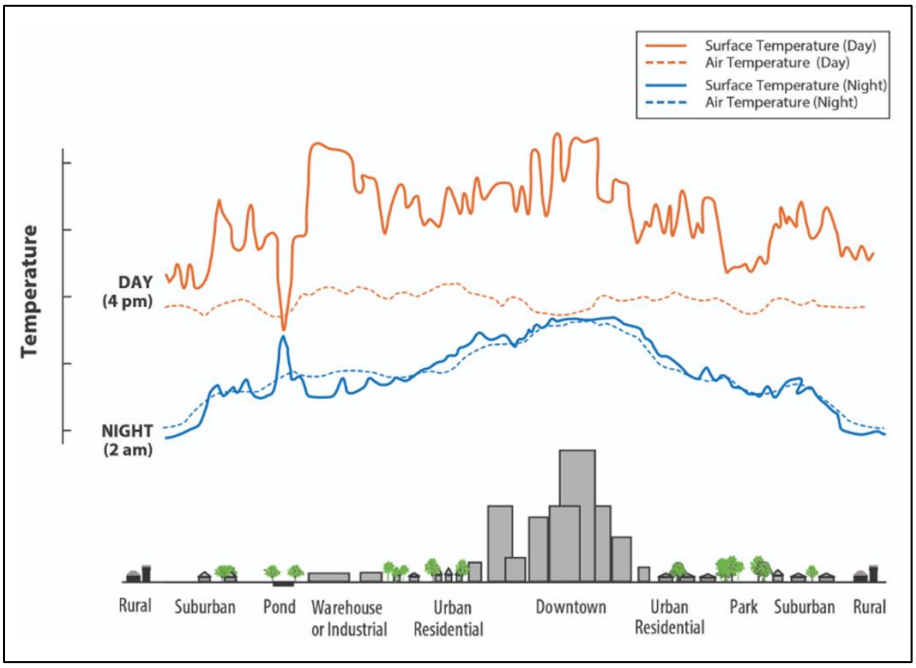

Figure 1: This image shows the temperatures of land surface and air during the daytime and nighttime over different land covers (EPA 2022c).

There are two main types of UHIs: surface urban heat islands (SUHIs) and atmospheric urban heat islands (Atmospheric UHIs). SUHIs are urban heat islands that "form because urban surfaces such as roadways and rooftops absorb and emit heat to a greater extent than most natural surfaces" (EPA 2022c). Atmospheric UHIs are similar but affect the local lower atmosphere around an urban area and use air temperatures instead of land surface temperatures. Research on UHIs and their impact on ecosystems, human health, and well-being are now common (for example: Yow (2007) and Sagris and Sepp (2017)). For example, people over the age of 65, under the age of 5, and with lung and heart issues/illnesses are disproportionately affected (EPA 2022b). To remediate the impact of heat islands, typical measures include increasing vegetation in those locations which can provide shade and have a cooling effect, or to build 'cooling centers' in communities located inside or nearby an UHI (EPA 2022a). However, research on SUHIs is less common, and especially their link to the thermal pollution of water.

SUHIs, the focus of this study, impact the environment when there are long or heavy rain events and flooding happens. The stormwater runoff is exposed to hotter land temperatures, increasing its temperature, which introduces thermal pollution to nearby rivers and streams. This pollution disrupts the aquatic ecosystems by potentially pushing inhabitants outside of their temperature optimal tolerance zone.

My research question is: is there a relationship between spatial patterns of warmer water temperatures and day-time surface urban heat islands in the lower Chesapeake Bay watershed within Virginia for the months of June, July, and August of 2019?

To address that question, I analyzed the months of June, July, and August because the summer months have hotter SUHIs due to the heat intensity. The objective is then to establish

whether there is a distance-based relationship between water temperatures and the location of SUHIs. Figure 2 illustrates the big picture and its relationships in a color-coded flowchart.

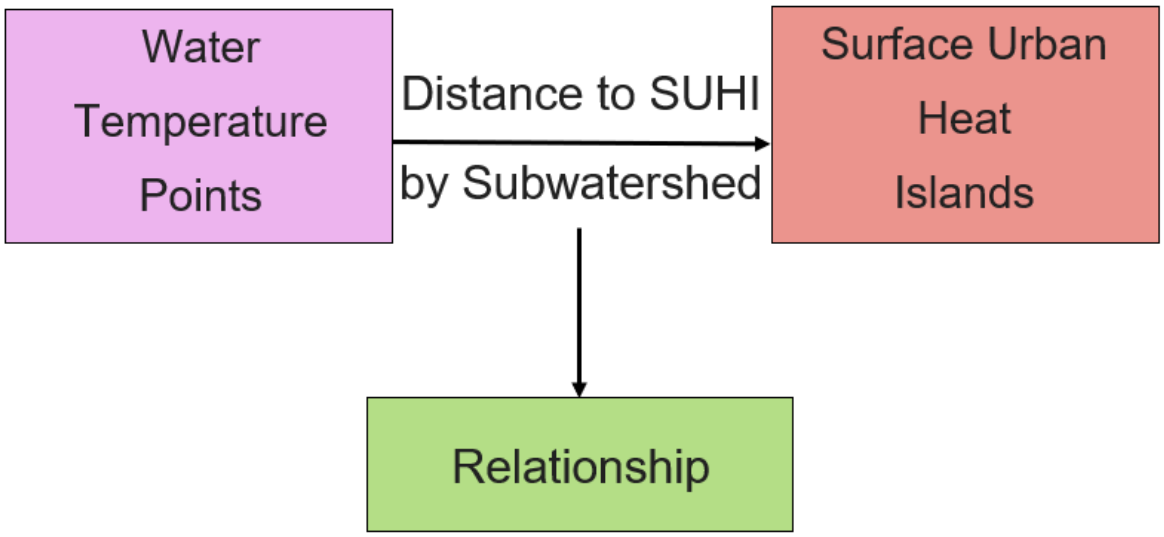

Figure 2: This color-coded flowchart shows the big picture components of this research study and how the water temperature points have been correlated with SUHIs in order to establish a distance-based relationship.

An EPA review of scientific studies found "the heat island effect results in daytime temperatures in urban areas about 1-7°F higher than temperatures in outlying areas and nighttime temperatures about 2-5°F higher" (EPA 2022c). Causes of these heat islands are reduced vegetated land covers in urban areas, urban material properties, urban geometry, heat generated from human activities, and arid weather conditions and lower topography. The thermal pollution introduced to nearby rivers, streams, lakes, and ponds "affects all aspects of aquatic life, especially the metabolism and reproduction… [and] can be particularly stressful, and even fatal, to aquatic life" (EPA 2022b).

Research on SUHIs and their link to water is important because it informs citizens and city planners/developers, and it highlights the impact an urban area may have on nearby water quality

and aquatic ecosystems. In addition, like in the case of UHIs, there is a social dimension to SUHIs as well: vulnerable, low-income communities are often more affected than higher-income communities (Huang and Cadenasso 2016). Higher awareness of both UHI's and SUHI's may push for more action towards reducing impervious surfaces within SUHIs by increasing vegetation, incorporating green roofs, and using materials that reflect heat when building new structures or renovating existing ones.

In this research study, I focus on the spatial relationship between SUHI locations and water bodies. One main assumption is that the closer water is to a surface urban heat island, the warmer the temperature of that water body is. That is, I expect a negative relationship between the distance from the station where water temperature was measured and the location of the SUHI. I also expect that relationship to be stronger if the measurement and the SUHI are within the same sub-watershed. Finally, I also expect the relationship to be stronger when the water measurement is downstream from the closest SUHI.

2. Literature Review

As mentioned above SUHIs are the focus of this study. In the following paragraphs I will cover environmental impacts (e.g., impacts of SUHIs on water pollution), human health impacts, economic impacts, related factors, remote sensing and GIS approaches, and local climate zones and their relationships with SUHIs.

2.1 Environmental Impacts of SUHIs on Aquatic Ecosystems

The main environmental parameter that this study looks into is water quality of nearby streams and rivers. One EPA study "found that urban streams are hotter on average than streams in forested areas, and that temperatures in urban streams rose over 7°F during small storms due

to heated runoff from urban materials" (EPA 2022b). When the temperature of water is affected, there is a chain of events that can happen. Warmer water temperatures decrease dissolved oxygen content, which negatively impacts survival of fish. Dead fish decompose, which generates excess nutrients in the water. Algal blooms then form to decompose the extra nutrients, and this decreases the dissolved oxygen content even further, creating a positive feedback loop (Harvey et al. 2011).

As a consequence, the aquatic ecosystem will be less diverse as native fish and other species are likely to get increased competition from invasive species, which are better acclimated to the higher temperatures (Kaushal et al. 2010). The health of land ecosystems is important for a healthy stream in return because if there is less vegetation, there are fewer trees to filter the runoff before it flows into the bodies of water. The "degree to which populations of freshwater species are affected by rapid increases in temperature will depend, in part, on their maximum thermal tolerance," which is "the temperature at which an organism loses the ability to maintain equilibrium" (Pagliaro and Knouft 2020, 2).

2.2 Human Health Impacts of SUHIs

There is a strong correlation between UHIs and SUHIs. In the presence of SUHIs, people feel higher temperature radiating from the urban surfaces and get heat-related illnesses like heat exposure/exhaustion (EPA 2022b). In addition, this heat influences car owners to drive instead of walking or using public transport because they want air conditioning. The increased use of vehicles diminishes air quality by introducing pollutants from the exhaust which stay in the air or precipitate. Those add to other car-related pollutants, like gasoline and coolant, and to land surface runoff, that flow into waterways further deteriorating environmental conditions. City residents are exposed to these air, land, and water pollutants more often which is especially

detrimental for people with asthma and other lung health issues. Air pollution also influences the water quality because water is a sink for carbon in the atmosphere. There are also studies that link increased human mortality rates from heat stress especially during heat waves, which are extreme in heat island locations. Heat related mortality can be caused by "respiratory failure and circulatory system failure from heart attack or stroke" (Tan et al. 2010, 80). Yow (2007) states that "heat kills more people than any other weather-related hazard, even in developed countries" (Yow 2007, 1237). For example, an article by Grothe and Lynch (2022) regards an extreme heat event on a hot summer morning at a baseball stadium where 8 attendees were sent to the hospital and over 80 others were treated for heat-related illnesses The event had to end prematurely and it had not yet hit the hottest time of the day.

2.3 Economic Impacts of SUHIs

There are negative economic consequences due to poor water quality and hot temperatures. Water and energy demand and consumption increase with the need for staying cool (Yow 2007, 1238). Emissions from using cooling energy affect the air temperature, which in turn influences the water temperature. Furthermore, warmer waters that affect fish populations impact fishing, both as a livelihood and a recreation activity. This applies to other businesses based on other water-based recreational activities that rely on good water quality such as kayaking, canoeing, paddle boarding, and swimming. Excess nutrients in water pollutants, combined with the higher water temperature, increase algae growth on the surface of water, which makes many of these activities harder or less appealing. The rivers and streams provide a scenic view to cities and towns, which drives up tourism and other linked industries like restaurants, shops, and lodging could also be impacted. For example, in Fredericksburg, VA, there are a lot of restaurants and

businesses overlooking the Rappahannock River for the appeal of the view of clean, healthy water along with a meal.

2.4 Related Factors for Water Temperature and SUHIs

The thematic contributions of literature within this field go into depth about how urban areas/land cover influence water temperature. Kaushal et al. (2010) looked at historical records showing water temperature for 40 sites. They found that 20 of the major streams and rivers experienced warming. The "annual mean water temperatures increased by 0.009-0.077°C yr-1 [(per year)], and rates of warming were most rapid in, but not confined to, urbanizing areas" (Kaushal et al. 2010, 461). This supports the message that increasing urban land cover impacts the temperature of water in the vicinity. They identify that the increases in stream water temperatures are usually due to increases in air temperature. This incorporates the UHI effect because it influences the air temperatures, the temperature people feel when walking around outside that has an impact on their health. Additionally, the impacts of increasing temperature in water are eutrophication, biological productivity, stream metabolism, contaminant toxicity, and loss of aquatic biodiversity, which supports the environmental impacts listed above in the substantive section of this literature review.

Water has a variety of properties and processes including specific heat capacity, latent heat exchange (evaporation and evapotranspiration), and depth profiles. The specific heat capacity of water is the amount of heat energy needed to raise the temperature of water; if the specific heat capacity is low, that means it does not take much heat to raise the temperature. Larger bodies of water like the Chesapeake Bay "have greater specific heat capacity and they have been found to provide a potential cooling effect during the daytime" (Wang et al. 2016). Additionally, with increasing urban land covers within cities that experience SUHIs, "vegetation and water surfaces

decrease and thus further reduce cooling effects caused by evapotranspiration [and]… this results in further heating of land surfaces and soil temperatures" (Schweighofer et al. 2021). There is a 'cold-skin' effect with water where the surface of water may be lower than the bulk temperature due to high evaporation and conduction losses (Noble and Jackman 1980). Water that is colder is less dense than warmer water, so it sits on the top and may affect water temperatures. The properties of water control its temperature.

To look into more of the ecosystem impacts of urban land cover, Paul and Meyer (2001) describe the changes caused by an increase in urbanization to streams and their landscape. The impervious surfaces alter the hydrology and geomorphology of the streams. These surfaces, along with runoff, increase the "loading of nutrients, metals, pesticides, and other contaminants to streams… [which] result in consistent declines in the richness of algal, invertebrate, and fish communities in urban streams" (Paul and Meyer 2001, 333). These environmental and biological changes emphasize the importance of understanding how a change in one environmental parameter can influence various other factors especially with the increase in urban land cover.

Nelson and Palmer (2007) address the anthropogenic stressors that alter water temperature, and these include increased watershed imperviousness, increased siltation, destruction of the riparian vegetation, and changes in climate. When water temperature is affected, there are impacts that happen in lieu of the change involving influences on ecological processes and stream biota. For example, "a profound community shift, from common cold and coolwater species to some of the many warmwater species currently present in smaller number, may be expected, as shown by a count of days on which temperature exceeds the 'good growth' range for coldwater species" (Nelson and Palmer 2007, 440). This has an effect on the food web as well. For their methodology, they looked at 5 different indices; (1) percentage of urban land cover in a

micro-watershed that drains to the site where data was taken, (2) total impervious surface within a micro-watershed, (3) total impervious surface in a buffer of 50 m on either side of the stream upstream from the site, (4) deforestation in a micro-watershed, and (5) deforestation within the 50 m buffer zone. Baseflow discharge was averaged, and water temperature was measured using Optic Stowaway Model WTA temperature loggers as well. The temperature surges they studied were linked to localized rainstorms, and they averaged to be about 3.5°C, dissipating over the duration of around 3 hours.

Cuba et al. (2019) explore the water-related downstream risks associated with mineral extraction. This relates to the downstream risk to waterways associated with SUHIs. They conclude that "many severe externalities of extractive development are experienced in areas hydrologically linked to the site of extraction, though these areas may not be those closest to mines themselves" (Cuba et al. 2019). This paper assists with understanding how downstream hydrology works and links it with environmental impacts.

Sechu et al. (2021) delineate the river valley bottom within drainage basins in Denmark using a cost distance accumulation analysis through GIS. Their tool "can delineate an area that has been the focus of management actions to protect waterways from upland nutrient pollution" (Sechu et al. 2021). The result of a cost distance accumulation is used to calculate the least cost path between two locations whether they be points, polygons, or lines. This shows one distance approach that can be done between water temperatures and their upstream SUHIs.

2.5 Remote Sensing and GIS Approaches to Study Urban Heat Islands

There are a variety of papers that use remote sensing data to identify urban heat islands. An early paper by Lo et al. (1997) used day and night airborne thermal infrared 5 m imagery from

the Advanced Thermal and Land Applications Sensor (ATLAS). The authors studied the thermal signature changes in urban land cover between day and night since UHIs absorb heat throughout the day and continue re-emitting throughout the duration of the night. They defined UHIs as a representation of the "human-induced urban/rural contrast," which supports this paper's use of the comparison of temperatures of the urban core with nearby agricultural areas to help identify UHIs (Lo et al. 1997, 287 and Yow 2007). They also include an additional examination of the relationship between land cover irradiance and vegetation amount by using NDVI. They found that "the predominance of forests, agricultural, and residential uses associated with varying degrees of tree cover showed great contrasts with commercial and services land cover types in the centre of the city, and favours the development of urban heat islands" (Lo et al. 1997, 287). They found that within their study area of Huntsville, Alabama, the highest irradiance (or thermal emission) during the daytime is in commercial land cover types while at night, the land covers are more homogenous from cooling down and have water being the land cover type with the highest irradiance.

In a more recent paper, Chen et al. (2006) go into depth about the relationship between UHIs and changes in land use/cover as cities are growing. Their study area is the Pearl River Delta in Guangdong Province, China, which is rapidly urbanizing. They use Landsat TM and ETM+ for temperatures and for the land use and land cover types. Their quantitative approach proposed a new index called normalized difference bareness index to extract bare land (NDBaI), which they compare with the normalized difference vegetation index (NDVI), normalized difference water index (NDWI), and normalized difference build-up index (NDBI). The correlations were found to be negative between NDVI, NDWI, NDBaI and the temperature while the correlation was found to be positive between NDBI and temperature. Their results showed that the UHIs were in

"a mixed pattern, where bare land, semi-bare land and land under development were warmer than other surface types" (Chen et al. 2006, 133). In addition, they found that vegetation is important for keeping an area cool in temperature because it provides shade that cools the local air temperature.

Clinton and Gong (2013) use MODIS (Moderate Resolution Imaging Spectroradiometer) and population data to "estimate the magnitude of thermal differentials urban heat islands and/or sinks, the timing of heat differential events, and the controlling variables" (294). They conducted a global study, but they focused on specific latitudes around the equator to see if arid cities had a hotter temperature for their potential SUHIs (as opposed to atmospheric UHIs). They constructed 5 and 10 km buffers around selected cities around the globe and found the surface urban heat by subtracting the surrounding temperature within the buffer from the core temperature of the city. Areas where the differential was positive were defined as SUHIs. The analysis included notable urban variables, which were ranked according to importance. They were: development intensity, vegetation amount, and size of the urban city/metropolis while the population number was the least important. Also, they found that arid regions had a higher temperature for the SUHIs in comparison to non-arid regions.

Zhou et al. (2019) produced a systematic review of the analysis of SUHIs studies using sensors like Landsat TM/ETM+/TIRS and Aqua/Terra MODIS from 1972 to 2019. In their study, China was the most studied region and summer daytime was the most frequent time period researched. The authors do point out the scarcity of nighttime UHI studies and highlight the ability of MODIS to collect thermal images that capture the energy emitted by Earth at night. They conclude that "the large spatial… and temporal… variations of SUHI are contributed by a

variety of factors such as impervious surface area, vegetation cover, landscape structure, albedo, and climate" (Zhou et al. 2019, 1).

In an earlier study that also looked at spatial and temporal patterns, Choi et al. (2014) assess SUHIs using cloud-free LST data that spans 1 year from the Communication, Ocean and Meteorological Satellite (COMS). The "LST was higher in low latitudes, low altitudes, urban areas and dry regions compared to high latitudes, high altitudes, rural areas and vegetated areas" (Choi et al. 2014). The study found that there is a maximum intensity of 10-13°C at noon during the summer with weaker intensities of 4-7°C during other times, especially nighttime, and other seasons. This article supports the finding that it is during the daytime in the summer when the SUHIs present the largest extent and intensities.

There are many factors that affect SUHIs and their intensity. SUHI "varies with latitude, climate, topography and meteorological conditions" (Haashemi et al. 2016). SUHI are more present at lower latitudes, dryer climates, lower elevations, and during heat waves or other hot weather with no rain. Yang et al. (2020) add in other factors such as cloud coverage, wind speed, and solar radiation. If it is cloudy, the sun's heat won't reach the land surface as strongly. Also, SUHIs develop more with higher inputs of solar radiation on the Earth's surface. Lastly, wind speed changes where SUHIs are; wind can blow hotter urban temperatures into a different area and cool down the urban land covers. Other factors to name are land cover, land use, morphology, structure and material of surfaces and buildings, human activity, and precipitation (Yang et al. 2020). Looking at these variables within a study area is important in order to consider all the processes affecting SUHI formations.

In what is probably the most influential paper for the present Capstone Project, Kaplan et al. (2018) synthesize the state of the art by stating that "UHI studies are generally conducted in two ways: through the air temperature measuring, or through measuring the surface temperature." The surface UHIs are extracted with the equation of "UHI = $\mu + \sigma/2$ in which μ is the mean LST value of the study area, and σ is the standard deviation of the LST" (Kaplan et al. 2018). Furthermore, the relationship of LST is found with NDVI and NDBI to see the trend; NDVI has a negative, or inverse, correlation with LST while NDBI has a positive, or direct, correlation with LST.

2.6 Local Climate Zones and their Relationship with SUHIs

Demuzere et al. (2021) introduces a methodology to obtain the local climate zones (LCZs) of a city or location. Benjamin Bechtel from the Bechtel et al. (2019) paper is an author of this paper as well. The concept of LCZs has been around since 2012, and it is explained in depth with its holistic classification approach. Training areas for the 17 classes of land cover are used in the LCZ Generator. Land classes 1-10 are urban areas (buildings and streets) while land classes 11-17 are natural areas (trees and water). The LCZ Generator outputs LCZ mapping and "simultaneously provides an automated accuracy assessment, training data derivatives, and a novel approach to identify suspicious training areas" to control for error (Demuzere et al. 2021). The LCZs classification system originally provided an UHI framework for studies.

Finally, using recent developments in the study of the relationship between land cover and temperature, Bechtel et al. (2019) use local climate zones (LCZs) to help identify SUHIs. LCZs are "a universal description of local scale landscape types based on expected variation at neighbourhood scale ($\geq 1km^2$) in and around cities." They use MODIS's and Landsat 8's LST multi-year average to compare to the LCZ scheme in 50 cities to investigate its suitability to

identify SUHIs. Both LST, which helps find SUHIs, and LCZs use some of the same variables that are important controls. The authors found that using an approach that combines LCZ and annual SUHI estimates provides a promising method for "a consistent and comprehensive SUHI analysis framework… to assess the spatial scale of matching LST and LCZ data, filter for topographic effects, and include the phenological status" (Bechtel et al. 2019).

2.7 Literature Review Conclusion

These papers helped me gain perspective and information about remote sensing and environmental responses from the water temperature. This research project looked at the correlation between water temperature in relation to its distance to the nearest SUHI within the sub-watershed. I expect a trend of warmer water temperature in locations where the distance to the nearest SUHI is shorter than the distances measured for cooler water temperatures. Use of Landsat data along with NLCD, NDVI, and NDBI were considered for this study from the input of these papers. LST, DEM, FD, and FA were additional variables incorporated in this project to incorporate land characteristics and water flow.

In this study, I use Landsat satellite imagery similar to Chen et al. (2006) and Zhou et al. (2019), NDBI and NDVI similar to Chen et al. (2006) and Lo et al. (1997), and land cover (or NLCD) similar to all of the remote sensing papers mentioned in the Remote Sensing and Urban Heat Islands section above. The chosen time period of this research is the late morning around 10:50 a.m. when Landsat 8 and 9 overpass the study area and the tiles of data selected are during the summertime because of the higher SUHI intensity mentioned in Choi et al.'s (2014) article. Kaplan et al.'s (2018) UHI equation is used to identify the SUHIs in the study area. Clinton and Gong (2013) and Nelson and Palmer (2007) both use the buffer method of distance between variables, which is one of the distance relationships considered but not used in this study.

Removing clouds from satellite imagery and using LCZs are utilized in this study, in the same way as shown by Bechtel et al. (2019). Also, the output of LCZs from Demuzere et al.'s (2021) methodology is used to see the built-up areas found to compare and validate the SUHIs identified. Furthermore, Kaushal et al. (2010) uses a simple linear regression to analyze their resulting trends/relationships. The gap I am filling is to test these combinations of methodologies for the lower Chesapeake Bay watershed.

3 Data and Methods

In this section, I go over the datasets utilized in this project along with the methods utilized to process and analyze them.

3.1 Data

The datasets (see Table. 1) used for this study can be organized in 3 groups: water station data, elevation data, thermal and land cover related data. The water station data includes the water temperature datapoints from the Chesapeake Bay Program (CBP), National Oceanic and Atmospheric Administration (NOAA), National Water Quality Monitoring Center (NWQMC), and Chesapeake Monitoring Cooperative (CMC) with many sub-sources such as USGS, Old Dominion University, Virginia Institute of Marine Science, Virginia Department of Environmental Quality, etc. (see Figures 4 and 5 for temporal and spatial coverage). Water depth is listed at some of the water stations but not all, which is recognized as an important environmental factor that cannot fully be taken into account in this study. Figure 6 shows the colored classes of water depth data and their spatial distribution. The elevation data is the DEM from USGS; Figure 13 shows the range of elevation within the study area. Finally, the thermal and land cover related data are: Bands 4, 5, 6, and 10 and cloud distance from Landsat 8 and 9

Collection 2 Analysis Ready Data (ARD) Level 2 scene tiles from USGS Earth Explorer; the NLCD from the Multi-Resolution Land Characteristics Consortium (MRLC); the national watershed boundaries (NBD) from the United States Geological Survey (USGS), Environmental Protection Agency (EPA), and National Resources Conservation Service (NRCS); and, the LCZs from Demuzere et al.'s (2022) global map of data. 26 Landsat tiles are used within the study area and its time duration. The LST, NDVI, and NDBI variables are calculated from the Landsat 8 and 9 bands while the FD and FA are derived from the elevation tiles. Most of the data is from the year of 2019 to keep it consistent with that summer's weather and ancillary data since the most recent NLCD dataset is from 2019. See Figure 16 for the spatial distribution of the 15 land cover classes. For the Landsat remote sensing imagery, the data are already processed and corrected for the atmosphere to be ready for direct use. The datasets were projected to NAD 1983 StatePlane Virginia South FIPS 4502 (Meters) to maintain angles and shapes.

Name	Source	Year	Format	Data Type	Resolution
Water Quality Station (Temperature)	CBP, NOAA, NWQMC, USGS	2019	Shapefile	Points	0.0001 m
National Land Cover Dataset (NLCD)	MRLC	2019	Shapefile	Raster	30 m
National Watershed Boundaries (NBD)	USGS, EPA, NRCS	2019	Shapefile	Polygon	0.0001 m
Landsat 8 and 9 C2 ARD L2 Satellite Imagery	USGS	2019	Tiff	Raster	30 m
Digital Elevation Model (DEM)	USGS	2019	Tiff	Raster	30 m

Local Climate Zones (LCZs)	Demuzere et al.	2022	Tiff	Raster	100 m

Table 1: This table shows the information regarding each of the data layers used for this research study. This includes its source, year, format, data type, and resolution. It is color-coded based on the big component it is used for (see Figure 2). This light purple is for the water temperature component, the light red is for the SUHI component, and the light green is for the relationship component between the two main variables.

The first component of this project focuses on the water temperature (Figure 3). The water temperature data is portrayed through a chart of measurement counts and maps of temperature (Celsius) and depth (meters) (Figures 4 through 6).

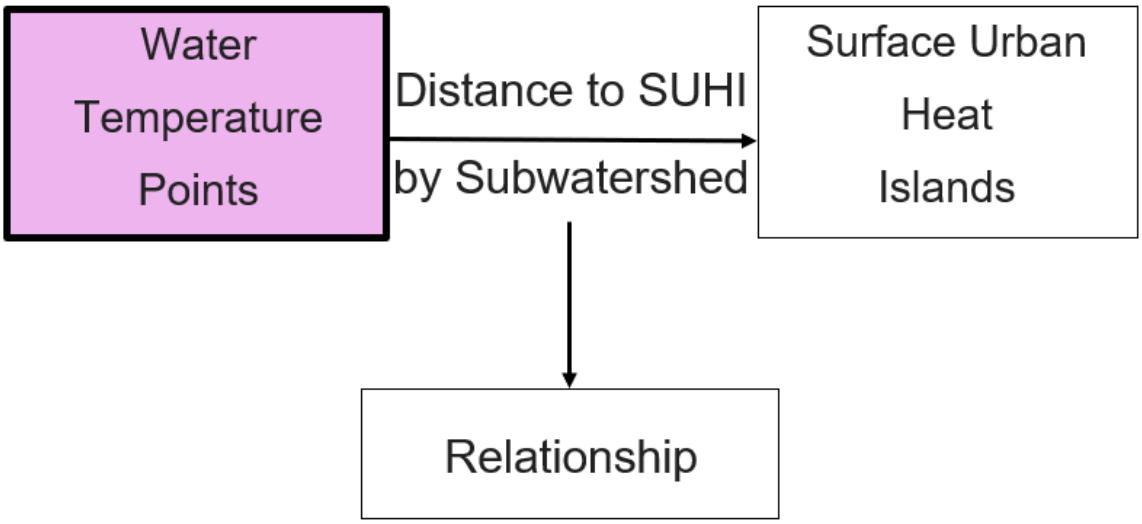

Figure 3: This flowchart highlights the water temperature component of this study.

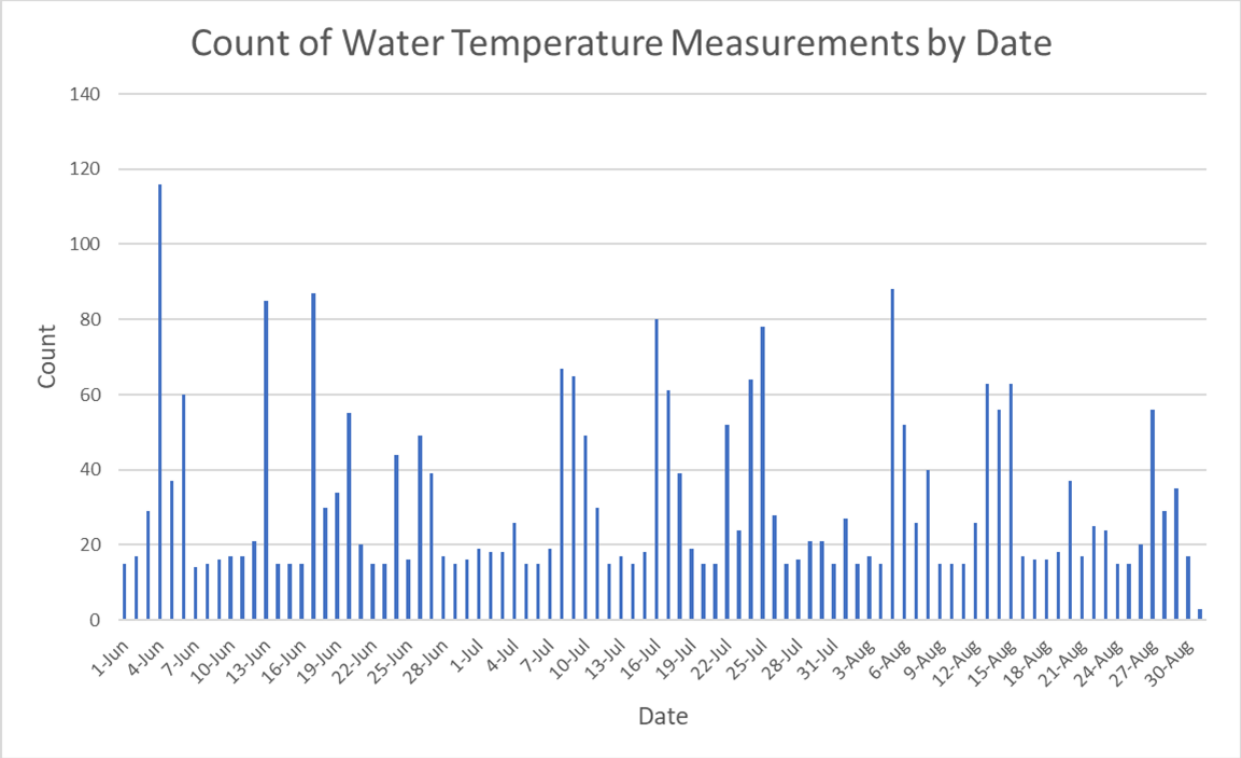

Figure 4: This bar chart shows the count of water temperature measurements by day across the study area for the summer of 2019. There are 2,818 measurements of water temperature across 25 sources total.

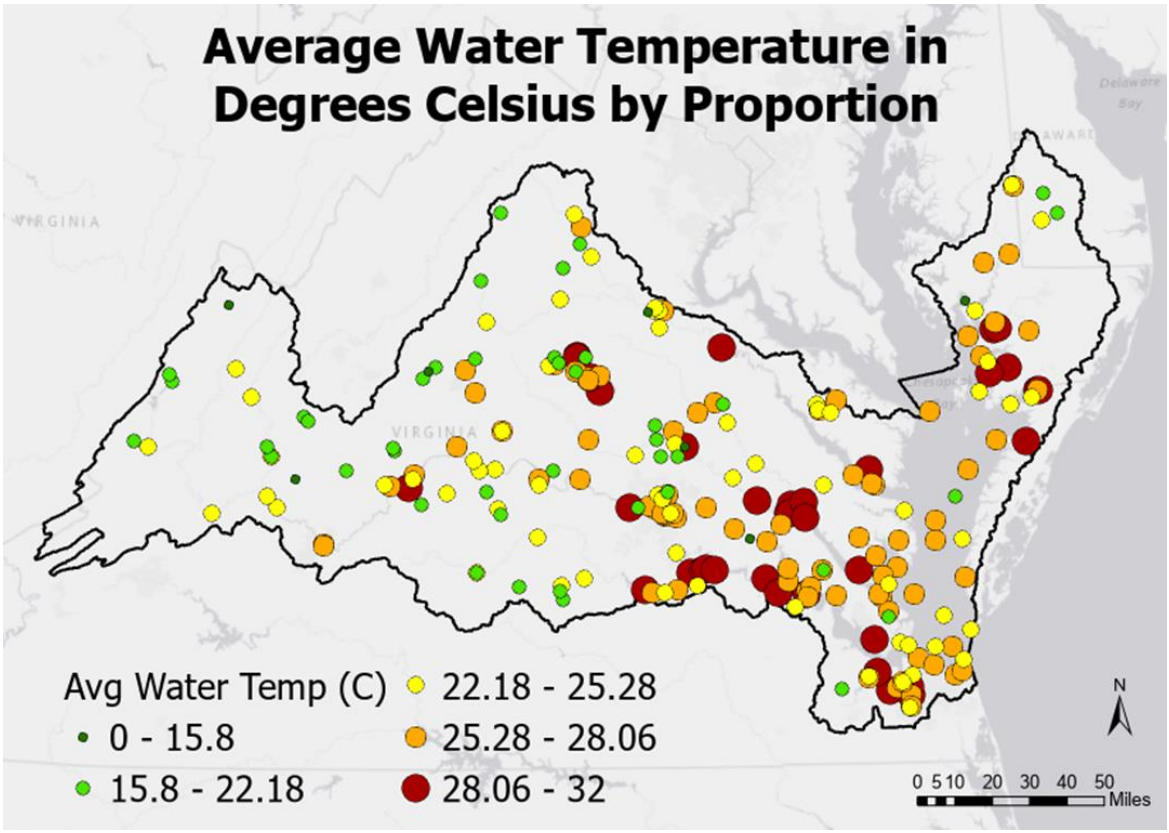

Figure 5: This map shows the outline of the study area in relation to the state of Virginia. It also displays the water temperature datapoints from the water quality stations obtained so far with classifications of temperature ranges in order to show the variation and warmer/cooler temperature values.

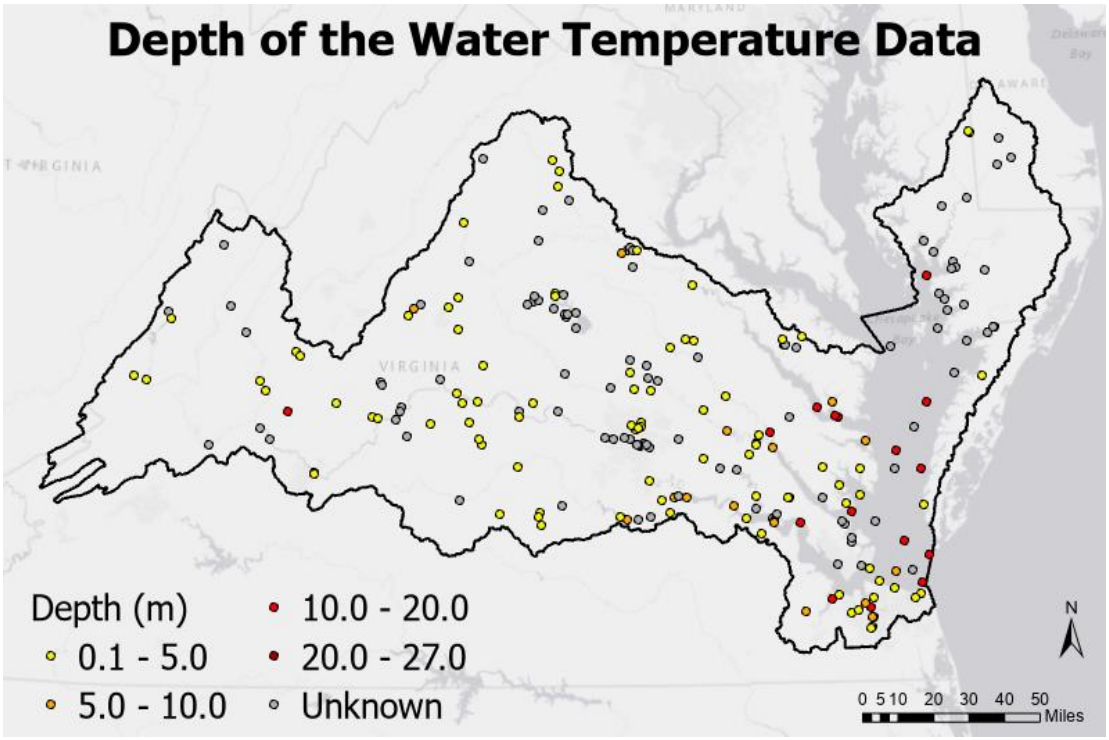

Figure 6: This map shows the depth of the water temperature measurements.

3.2 Methods

For this project I used three approaches to evaluate the relationship between the water temperatures and the SUHIs. Each approach is progressively more complex. The first approach is finding the relation of water temperature at zero distance; this is comparing the water temperature points that are contained within a SUHI to those outside of it. The second approach is omni-directional distance meaning that the distance between a water temperature point and its nearest SUHI is found whether it is upstream or downstream. Lastly, the third approach is uni-directional with the water temperature point's nearest SUHI being only upstream from it (i.e., the water temperature measured is downstream from the nearest SUHI). The third approach is more complex in finding the measurements.

The flowchart in Figure 7 describes the overall data processing and analysis steps I performed for this project. The following section describes those steps in more detail.

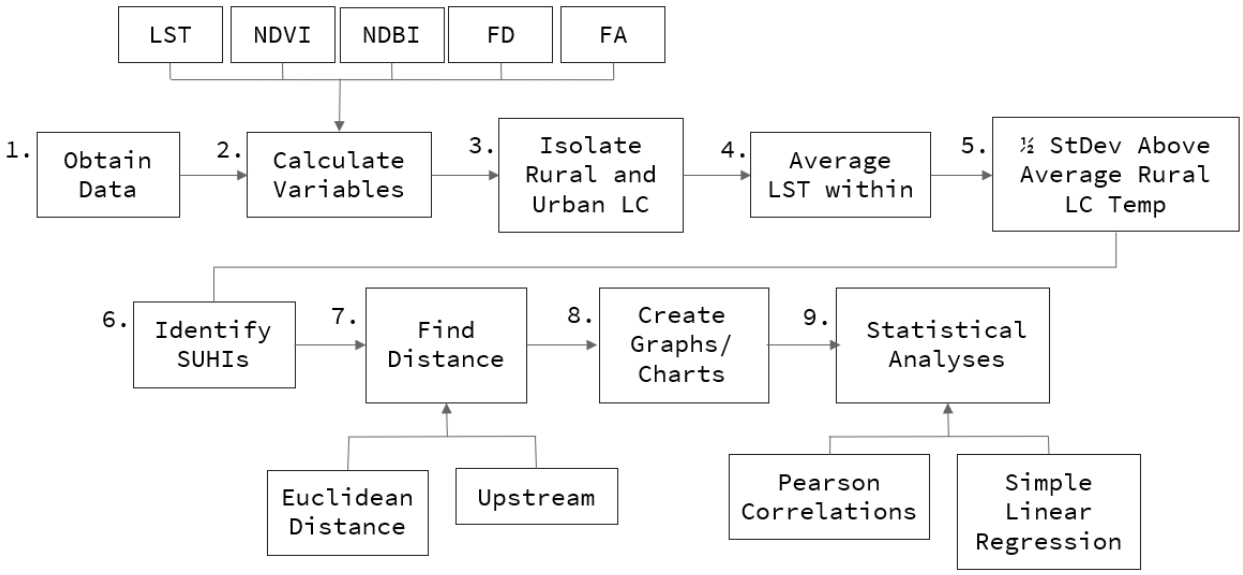

Figure 7: This flowchart shows the overall step-by-step process of the methodology to find the outcome of the relationships between water temperature and distance to SUHIs.

The GIS methodology for steps 1 through 6 in Figure 7 identify SUHIs, which is the second big component of this research (Figure 8).

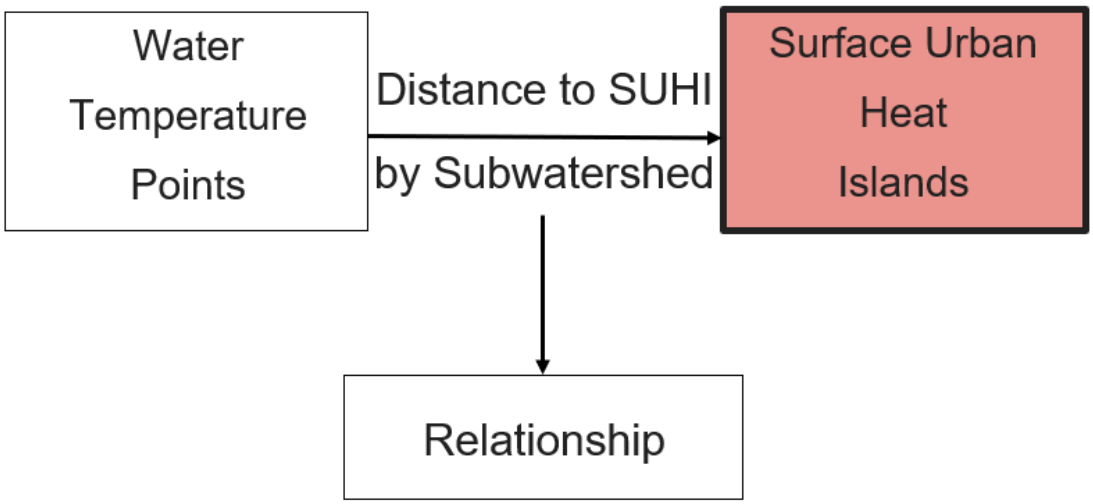

Figure 8: This color-coded flowchart shows the big component of SUHIs within this study.

3.2.1 Flowchart Steps 1 and 2

First, all data was collected and projected to NAD 1983 StatePlane Virginia South FIPS 4502 (Meters) to reduce uncertainty in calculations derived from mismatched projections. Next, the LST, NDVI, and NDBI were calculated using the raster calculator tool in ArcGIS Pro. Specific formulas are described in the following paragraphs.

Celsius = ((Multiplicative Scale Factor * Thermal Band 10) + Additive Offset) - 273.15, or C = ((0.00341802 * B10) + 149.0) - 273.15 for the case with Landsat 8 and 9 (USGS 2022). Figure 9 shows the processed data which displays spatial distribution of land surface temperatures (LST) in Celsius for the study area. Figure 10 displays the histogram showing this distribution of LST.

NDVI was calculated using the near infrared (band 5) and red (band 4) bands and the following equation of (NIR B5 - Red B4) / (NIR B5 + Red B4). Figure 11 shows the processed data and its spatial patterns.

NDBI was calculated with the middle infrared (band 6) and near infrared (band 5) bands and the following equation of (MIR B6 - NIR B5) / (MIR B6 + NIR B5). Figure 12 shows the processed data and its spatial distribution.

The flow FD and FA variables were calculated with the DEM. The DEM was input into the Flow Direction tool and that output was used as input into the Flow Accumulation tool in ArcGIS Pro. Figures 14 and 15 display those spatial distributions.

The distance to shore (m) was calculated with the sub-watershed boundary of the Chesapeake Bay within the study area. This variable was used to visualize if there was a correlation between water temperature and distance to shore. The Euclidean Distance tool was used to obtain the distance values to the nearest shoreline.

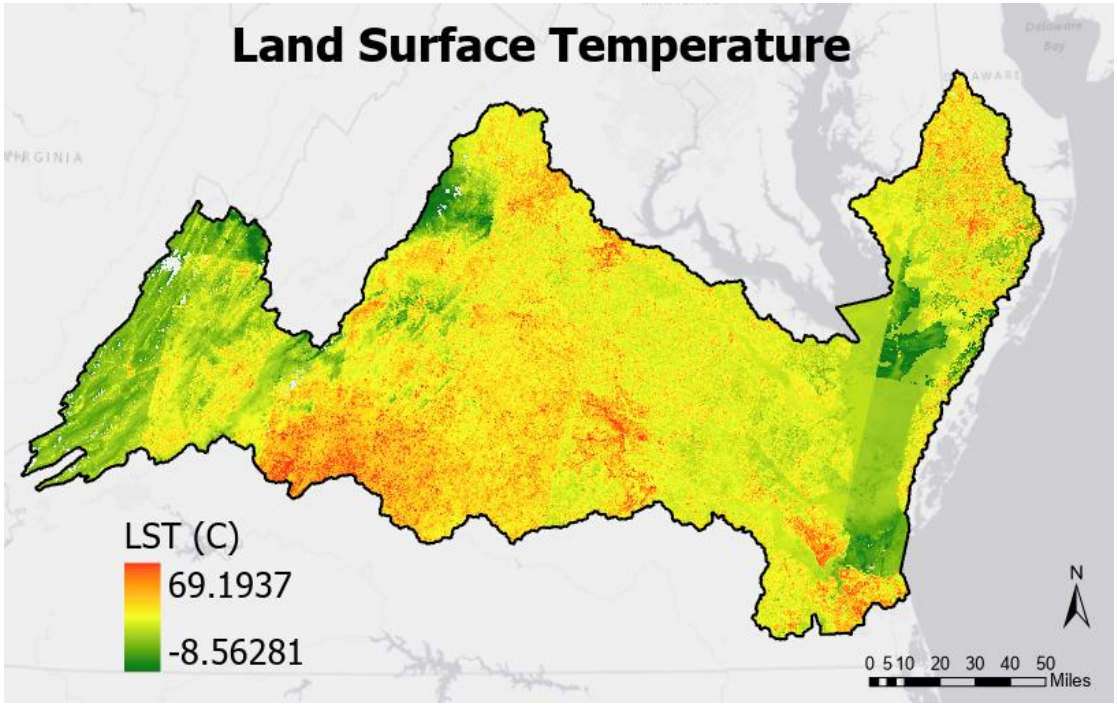

Figure 9: This map shows the land surface temperature for the study area using thermal band 10 from Landsat 8 and 9. Thermal band tiles are averaged for the summer of 2019 with some band tiles from the summer of 2018 to fill in data gaps in the Virginia Beach area.

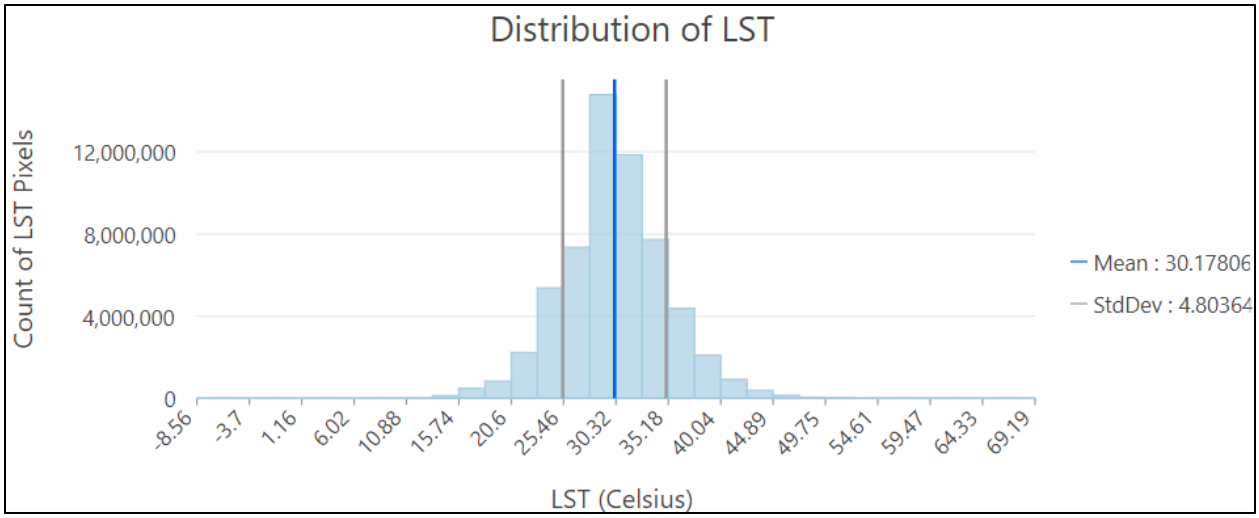

Figure 10: This histogram shows the distribution of LST along with its mean and standard deviation.

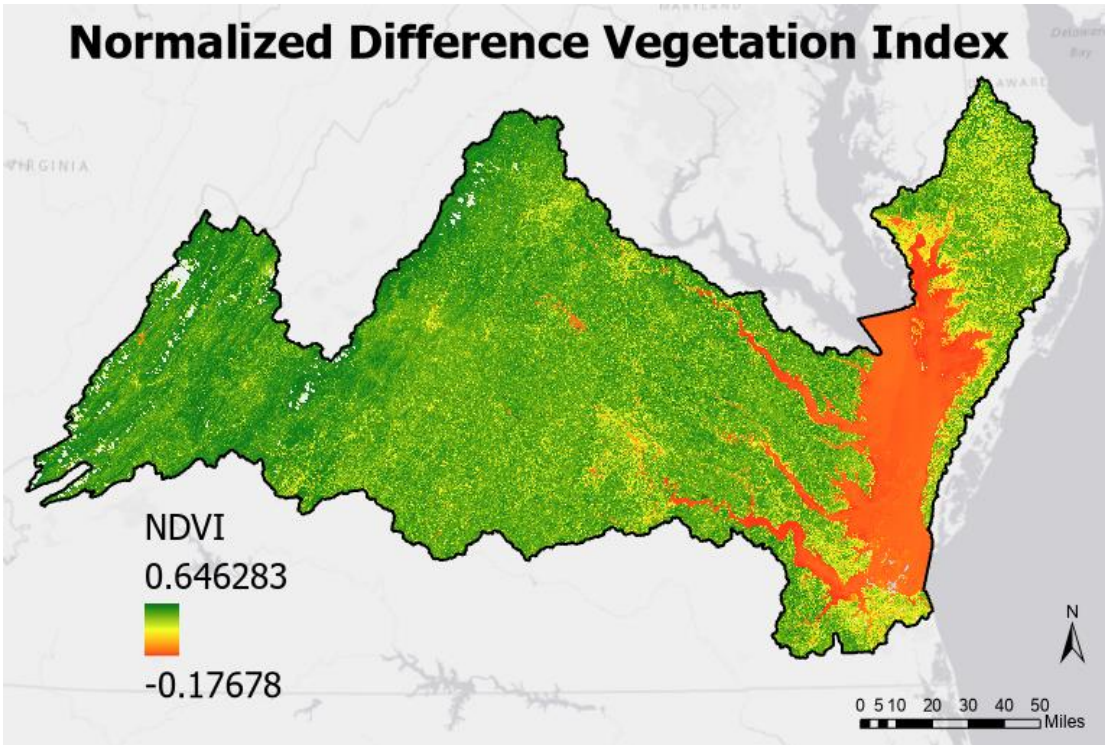

Figure 11: This map shows the normalized difference vegetation index for the study area. The higher the positive value, the more healthy, green vegetation there is.

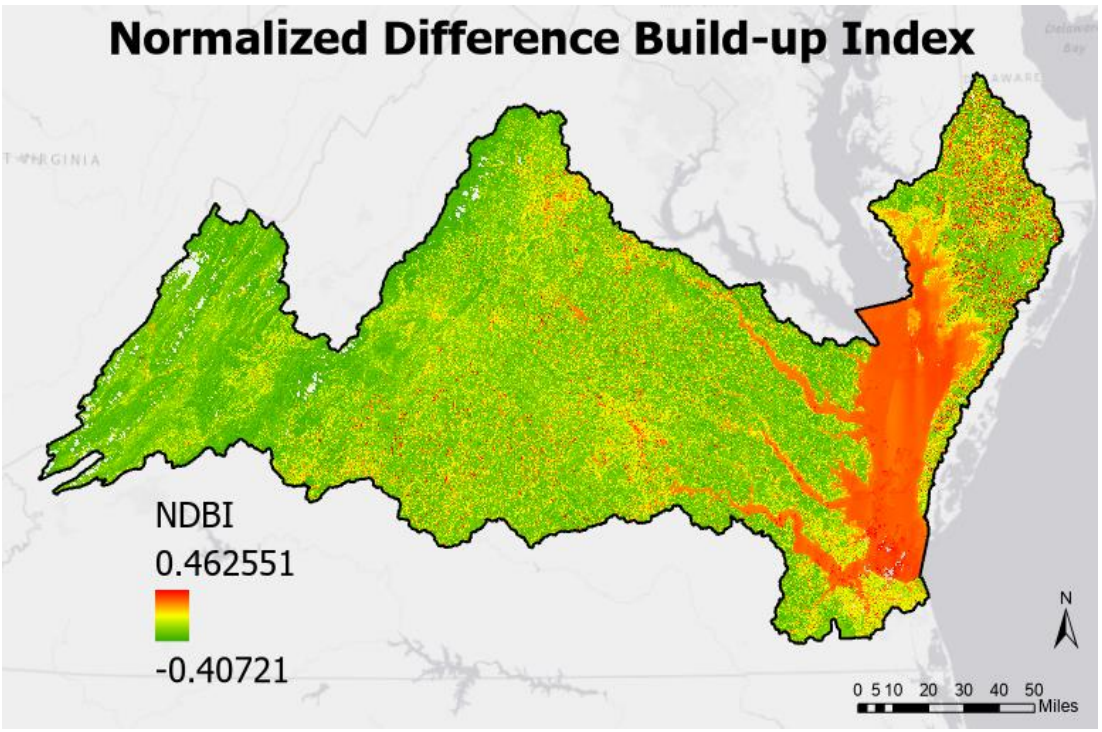

Figure 12: This map shows the normalized difference build-up index for the study area. The higher the value, the more built up, or urban, the land is with the exception of water.

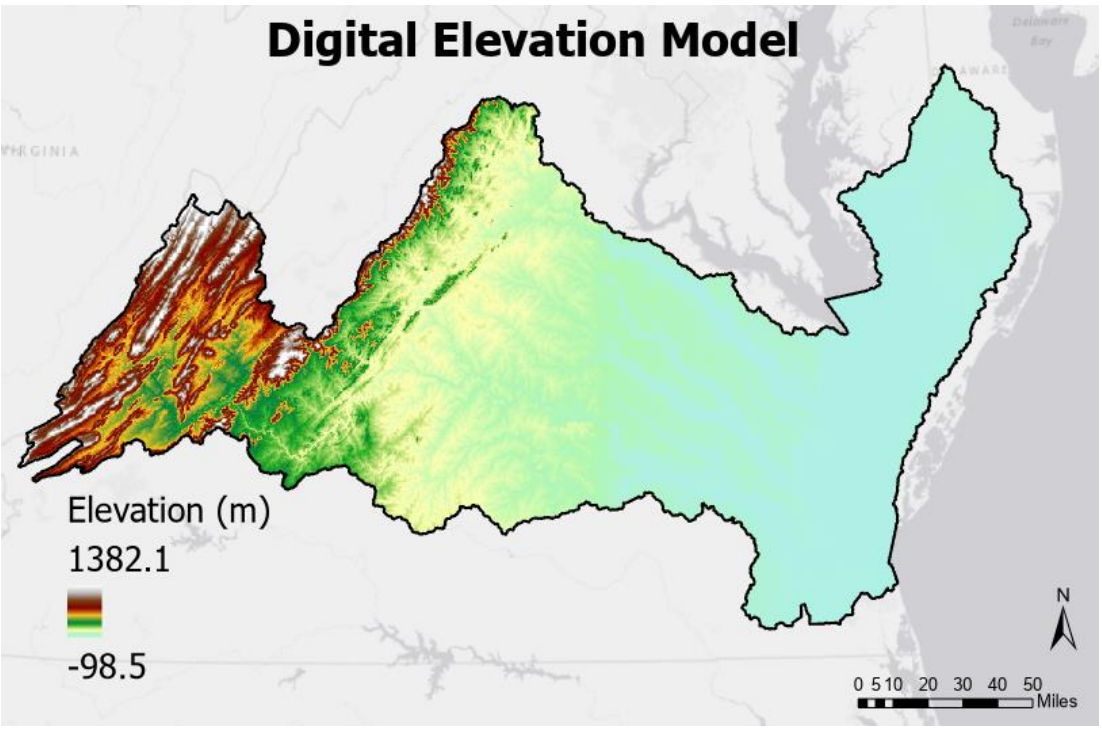

Figure 13: This map shows the elevation of the study with the Shenandoah Mountain range in the west and the flat coast in the east.

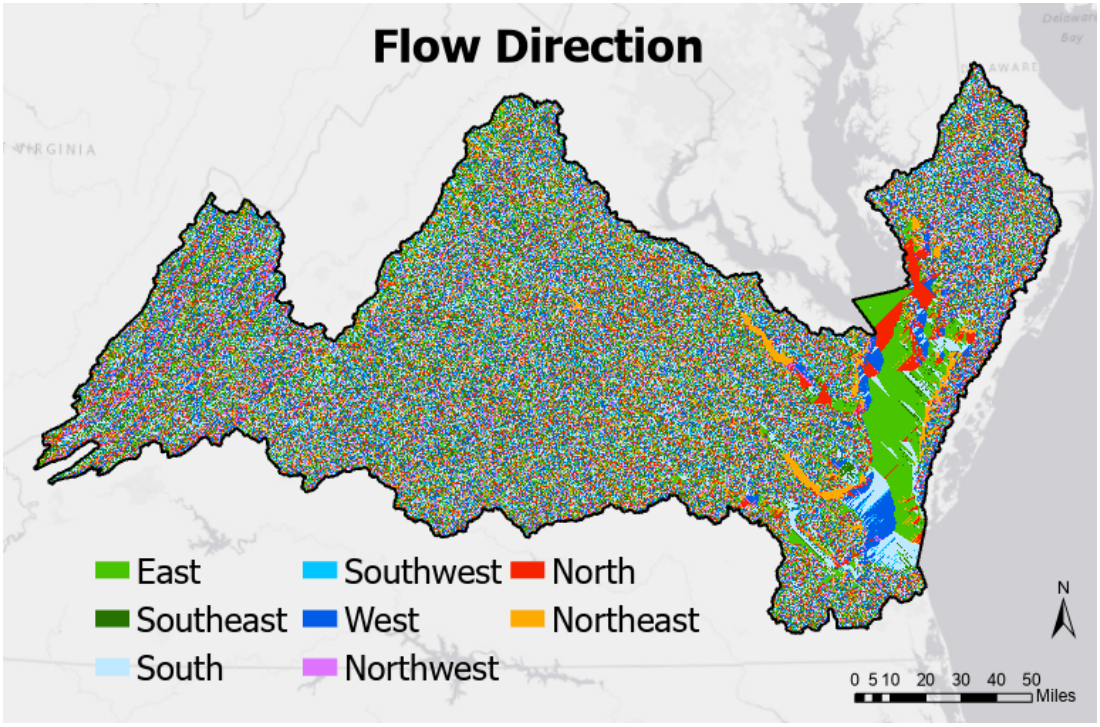

Figure 14: This map shows the flow direction calculated from the elevation surface.

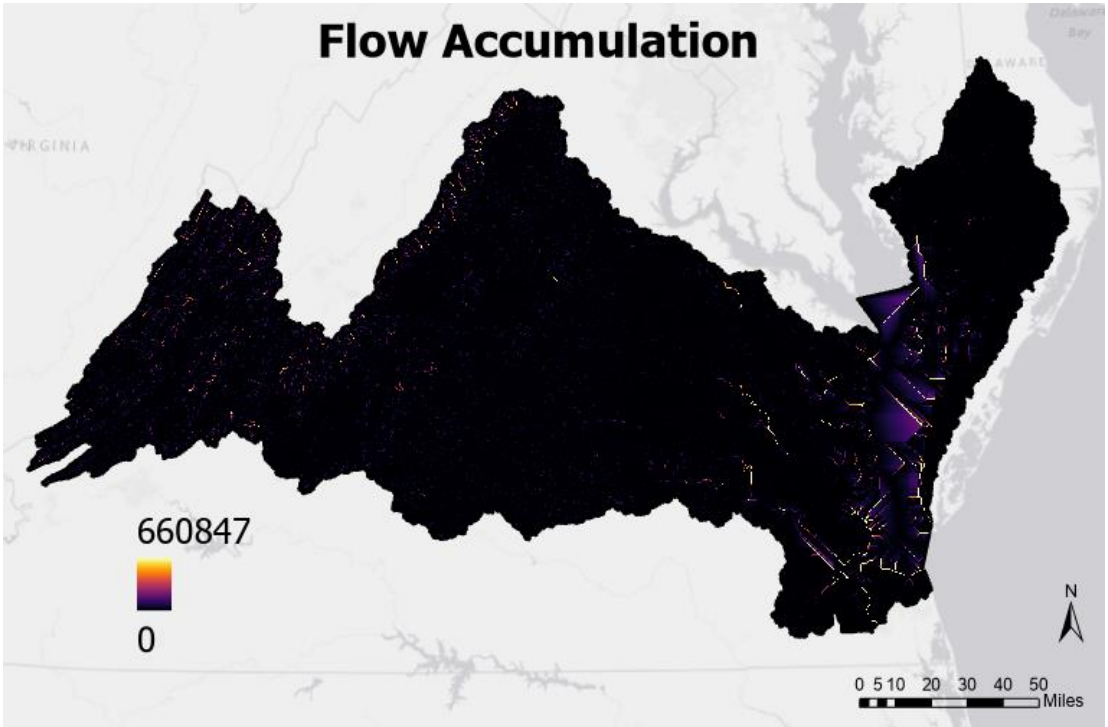

Figure 15: This map shows the flow accumulation calculated from the elevation surface. The streams and rivers flow into the Chesapeake Bay.

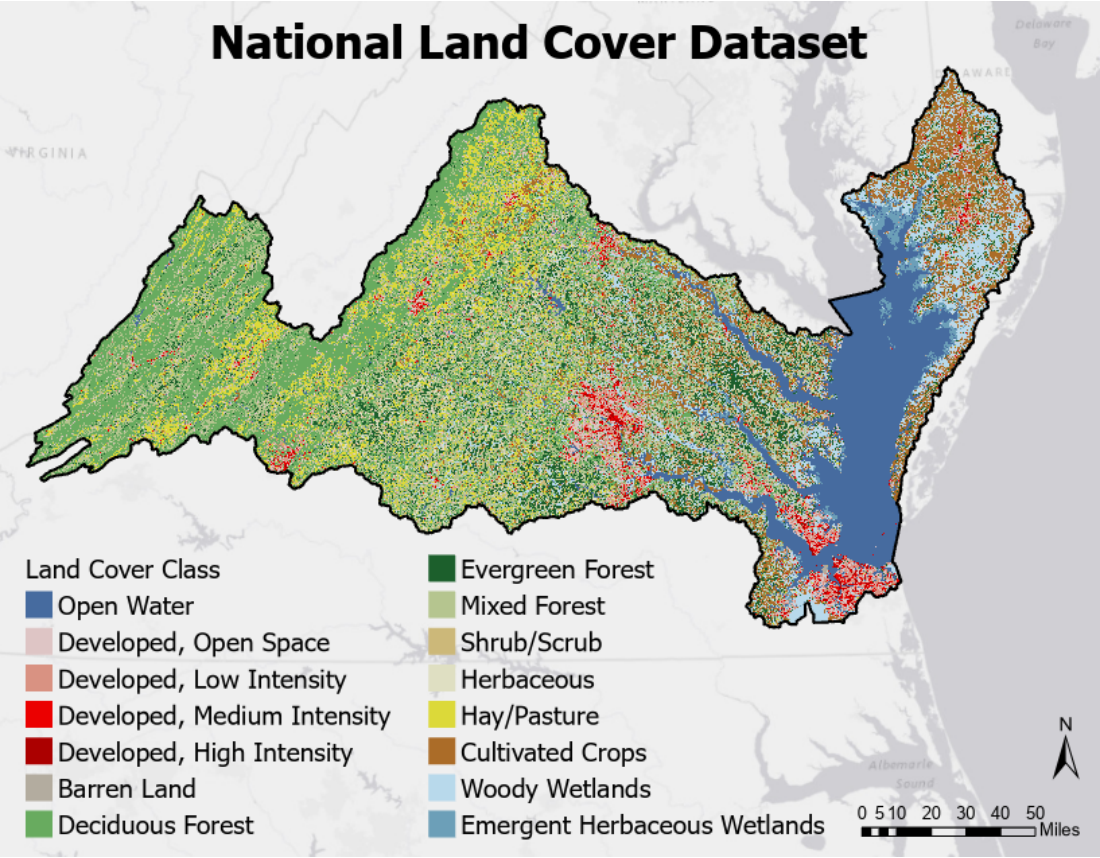

Figure 16: This map shows the 2019 land cover categories from the National Land Cover Dataset for the study area.

3.2.2 Flowchart Steps 3 through 6

The average LST of the study area for agricultural land cover (cultivated crops and hay/pasture classes) was calculated by isolating the agricultural land covers into their own polygons with the raster to polygon tool then selecting the rural land covers to export the data into its own feature class. Next, the ArcGIS Zonal Statistics as Table tool was used to find the mean LST for the agricultural land cover polygons. As mentioned in the beginning of this paper, SUHIs are identified by comparing the temperature of urban land cover with their surrounding

rural land covers. Any LST over a half a standard deviation above the rural temperature average within the study area is an area that has hotter temperatures than its surrounding agricultural land cover (Kaplan et al. 2018). Figure 17 shows the spatial distribution of SUHIs derived from the calculations described.

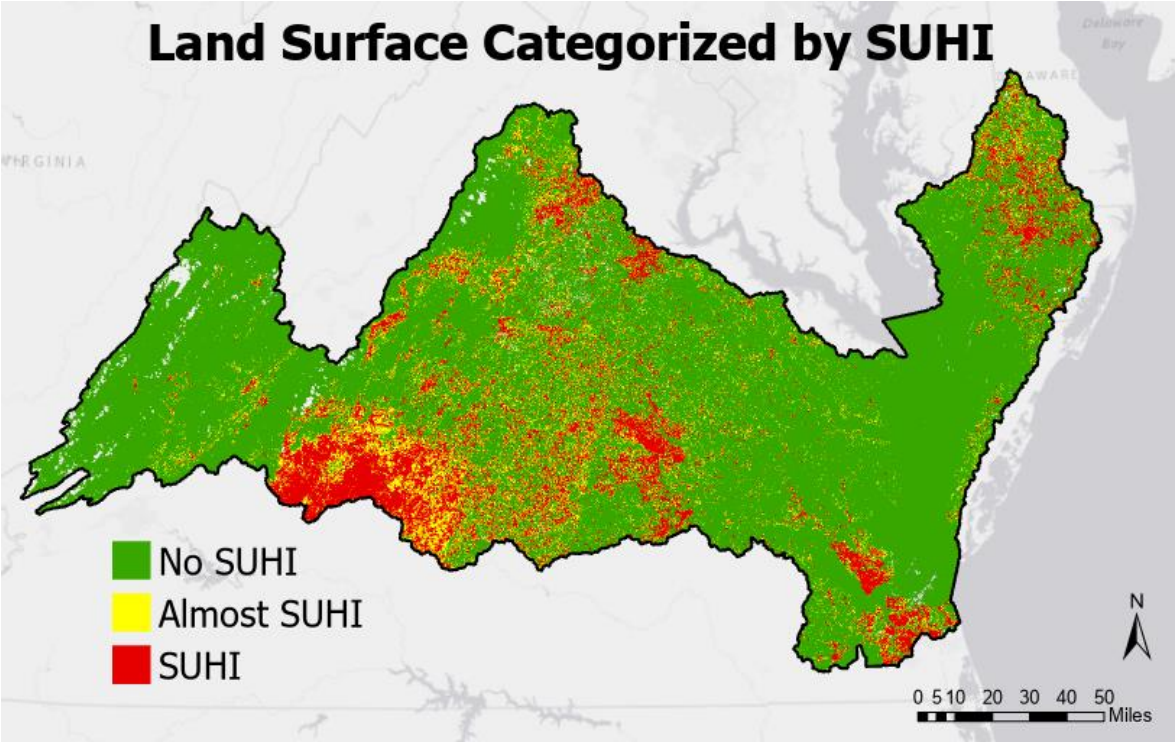

Figure 17: This map shows the identified surface urban heat islands as defined by Kaplan et al. (2018) in red, which means the LST is half a standard deviation above the agricultural land cover LST average. The areas with LST temperatures above the agricultural land cover LST average but below the half standard deviation above that average are in yellow. The areas with no surface urban heat islands and LSTs under the agricultural land cover LST average are in green.

Local climate zones (LCZs) can be used to see which areas that are classified as built-up coincide with the SUHIs (Bechtel et al. 2019). This is a form of validation for determining whether SUHIs are in areas that are likely to be urban heat islands. This study uses the LCZs created from Demuzere et al.'s (2022) global map of LCZs which was downloaded. A detailed

flowchart of the steps performed is shown in Figure 18. A description of those steps follows in the next paragraphs.

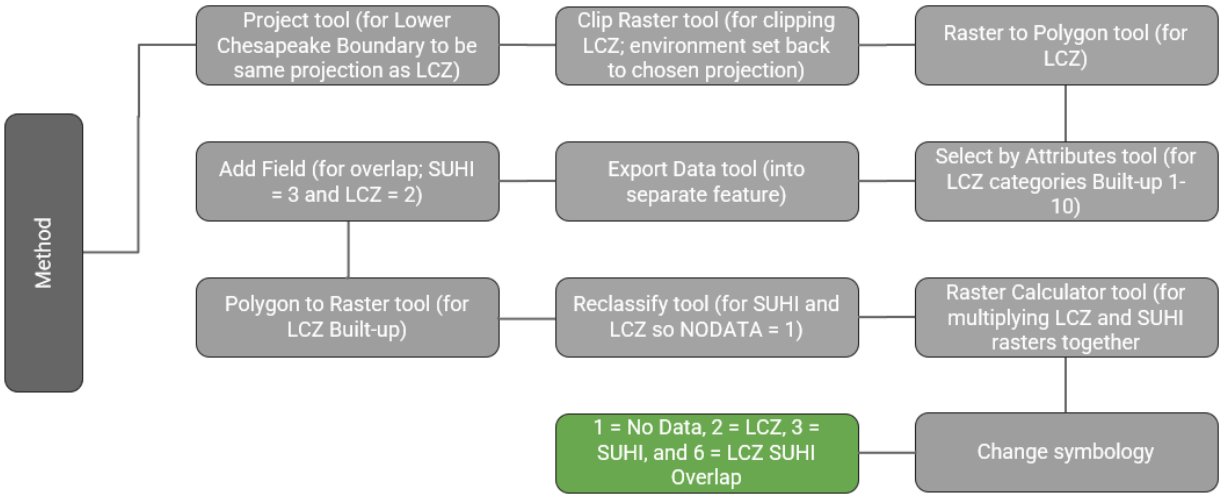

Figure 18: This flowchart shows the workflow of defining the overlap between surface urban heat islands and local climate zones.

The study area boundary feature class is projected to the same projection as the LCZ raster since the raster data is too large with the extent being the whole globe; this way the project tool runs faster. The environment settings for all tools automatically goes to the same NAD 1983 StatePlane Virginia South FIPS 4502 (meters) coordinate system, so when the clip raster tool runs, it automatically projects back to the selected coordinate system. Next, the land classes as a raster are converted into polygons with the raster to polygon tool in order to select only urban land classes 1-10 with the select by attribute tool. The selected features are then exported into their own feature class using the export data tool. A field in the attribute tables is added for the SUHIs being the value of 3, the urban LCZs being the value of 2. The urban LCZ polygons are converted back to a raster with the polygon to raster tool so that they can be reclassified with the reclassify tool for the ‘no data area to be equal to the value of 1’. The already rasterized SUHIs

are also reclassified to get the 'no data areas to be values of 1'. Figure 19 shows the spatial distribution of LCZs cropped for the study area.

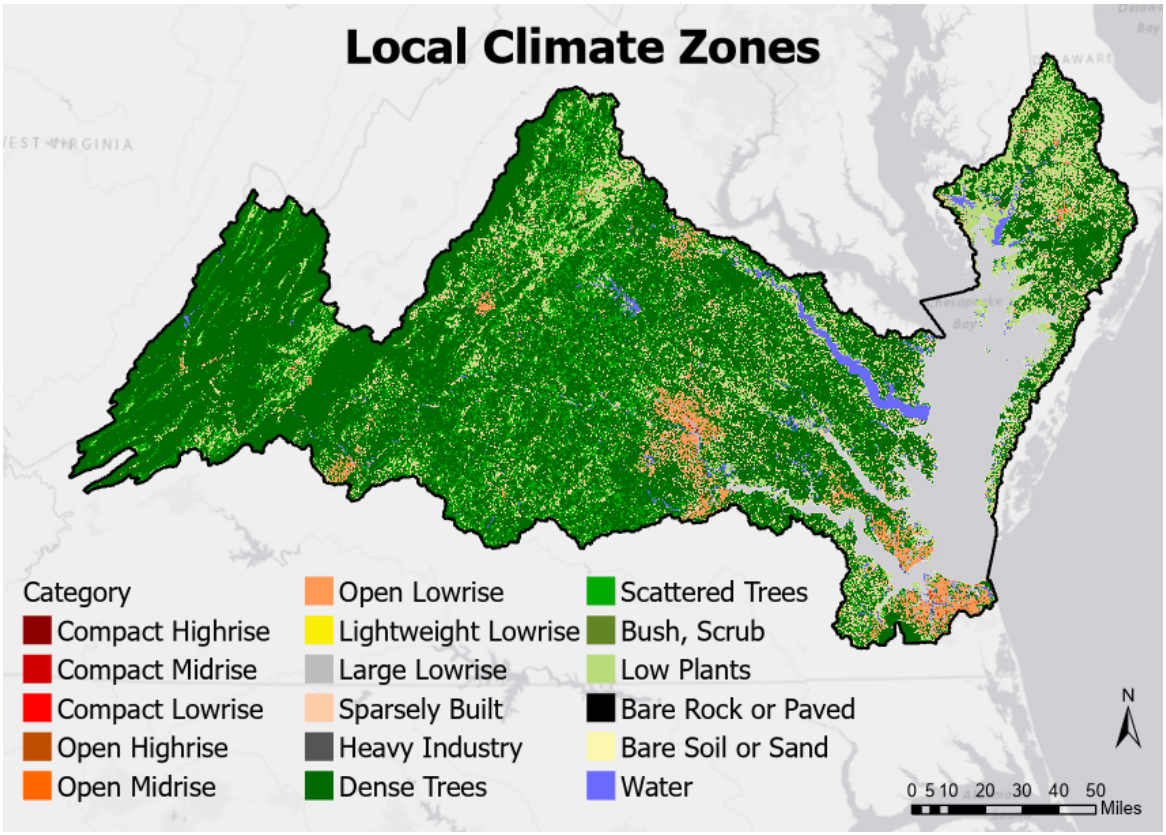

Figure 19: This map depicts the different land classes of the local climate zones within the study area. The first ten classes are urban land covers (compact highrise through heavy industry) and the last 7 classes are natural land covers (dense trees through water). The urban land classes are related to the areas with SUHIs.

Next, the raster calculator tool is used to multiply the urban LCZs and SUHIs together in order to get the values of where there is no data, an overlap, and no overlap between the two variables. The output values were then labeled 1 = no data, 2 = urban LCZ, no SUHI, 3 = SUHI, no urban LCZ, and 6 = overlap between urban LCZ and SUHI. The combine tool between the urban LCZs and SUHIs was used to compare the maps from Figure 17 and 19 (only urban/built-up classes). The overlap between urban/built-up LCZs and SUHIs shows that there are areas of agreement between the two approaches. Areas of agreement (label 6) can be interpreted as

SUHIs with less levels of uncertainty. SUHIs with no overlapping urban/built-up LCZs can be interpreted as having less certainty. One interpretation of the source of uncertainty in the definition of those non-overlapping SUHIs is the influence of weather like rain or drought events. Non-overlap areas are notoriously clustered in non-urban areas in the south central to west boundary area (areas in yellow in Figure 20).

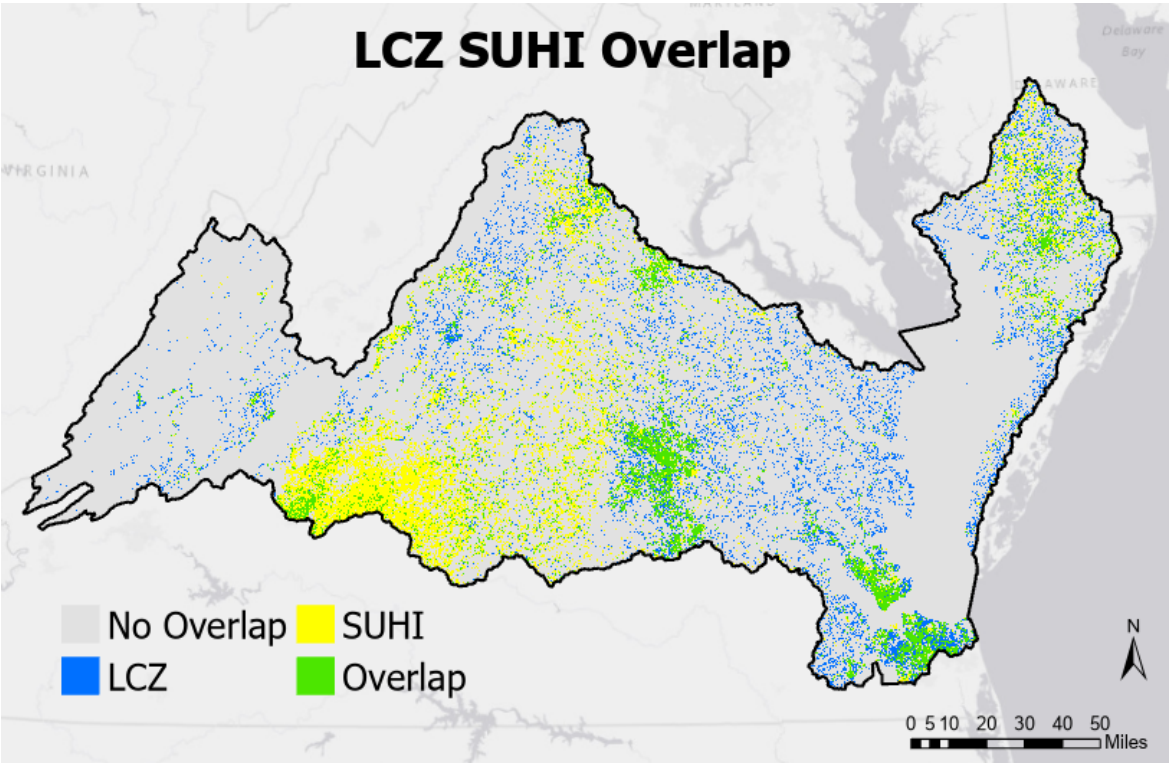

Figure 20: This map shows the comparison between surface urban heat islands and local climate zones. The yellow polygons are where there is only SUHIs; the blue polygons are where the urban LCZ land classes are; the green polygons are the overlap where the SUHIs and urban LCZ land classes coincide; and, the gray area is where there is neither SUHI or urban LCZ land classes.

While I kept an expansive/inclusive or liberal definition of SUHIs like the one displayed in Figure 17 (with both overlap and no overlap with LCZ) for the rest of the analysis presented in this paper, it is worth noting that the decision may have had an impact in the results discussed later in this paper. I will return to this point in the discussion section of the paper.

Figure 21 shows the third and last big component of this study: the relationships between water temperature and SUHIs. This is explained in Steps 7 through 9.

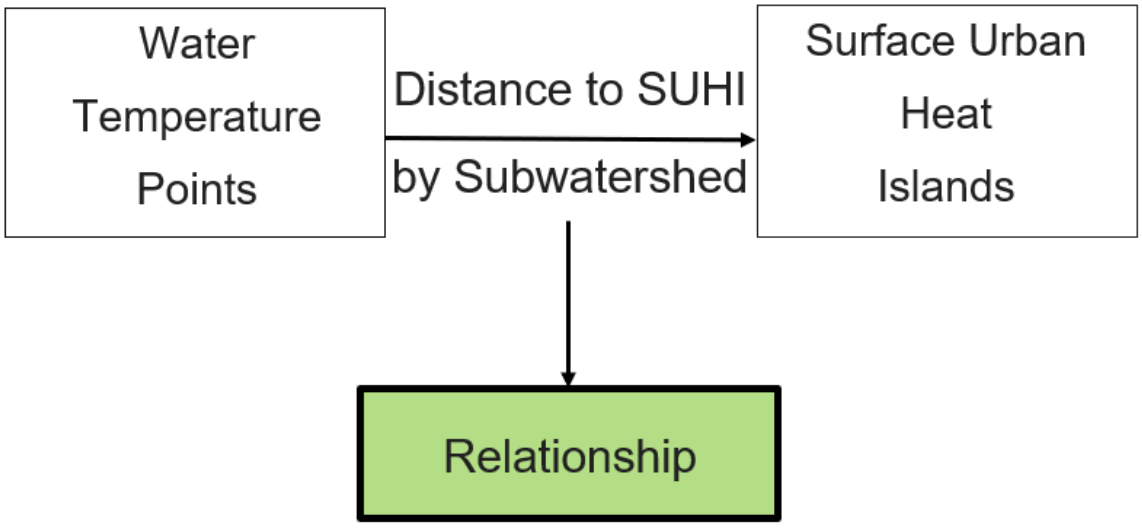

Figure 21: This color-coded flowchart shows the big component of the distance relationships within this study.

3.2.3 Flowchart Step 7

Now that the SUHIs are identified, the different approaches to distance between the water temperatures and nearest SUHI can be calculated. As explained earlier, several approaches with subsequent levels of complexity were attempted. In general, I relied on Euclidean Distance and Direction Distance tools. I restricted the calculations to each sub-watershed's boundaries because the runoff from the SUHIs flows downstream within them. The distance between water temperature points and the nearest SUHI were not restricted within the sub-watershed when the measurement point was located within a river's tidal section because there are many sub-watersheds upstream that flow into the river.

For the first approach, the distance-zero approach, two ways were available to establish whether the water temperature points were contained within a SUHI or not. Both are described in

Figure 22. The first way requires the omni-directional Euclidean distance tool, which outputs a raster surface that depicts distance away from the closest SUHI for each pixel (see Figure 23). Then, the extract multi values to points tool is run in order to assign distance values to a field in the attribute table of the water temperature points. Then, the select by attributes tool is used on that field to select the Euclidean distances that are at 0 meters (i.e., are contained within a SUHI); the reverse selection provides the water temperature points that are not contained within a SUHI. A new attribute table field us then created that classifies whether the water temperature point is contained within a SUHI or not. The second way to identify distance 0 or water temperature points contained within a SUHI is to use the intersect tool.

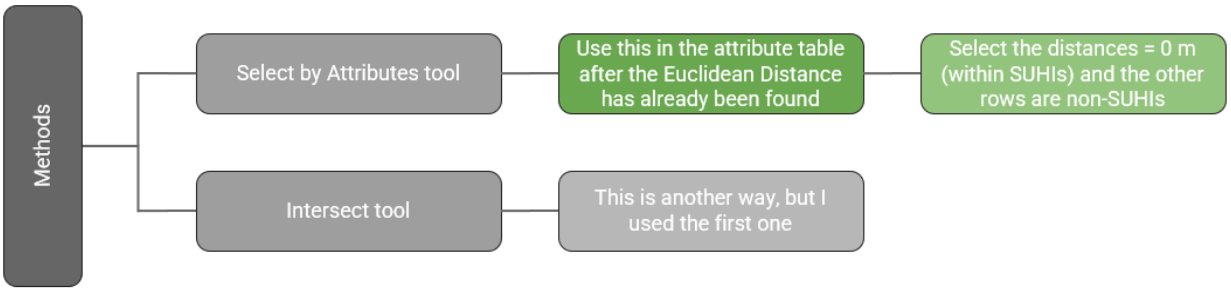

Figure 22: This flow chart shows the first distance approach's workflow. There are two methods to finding the no-distance between water temperature points and SUHIs; the first option is used in this case.

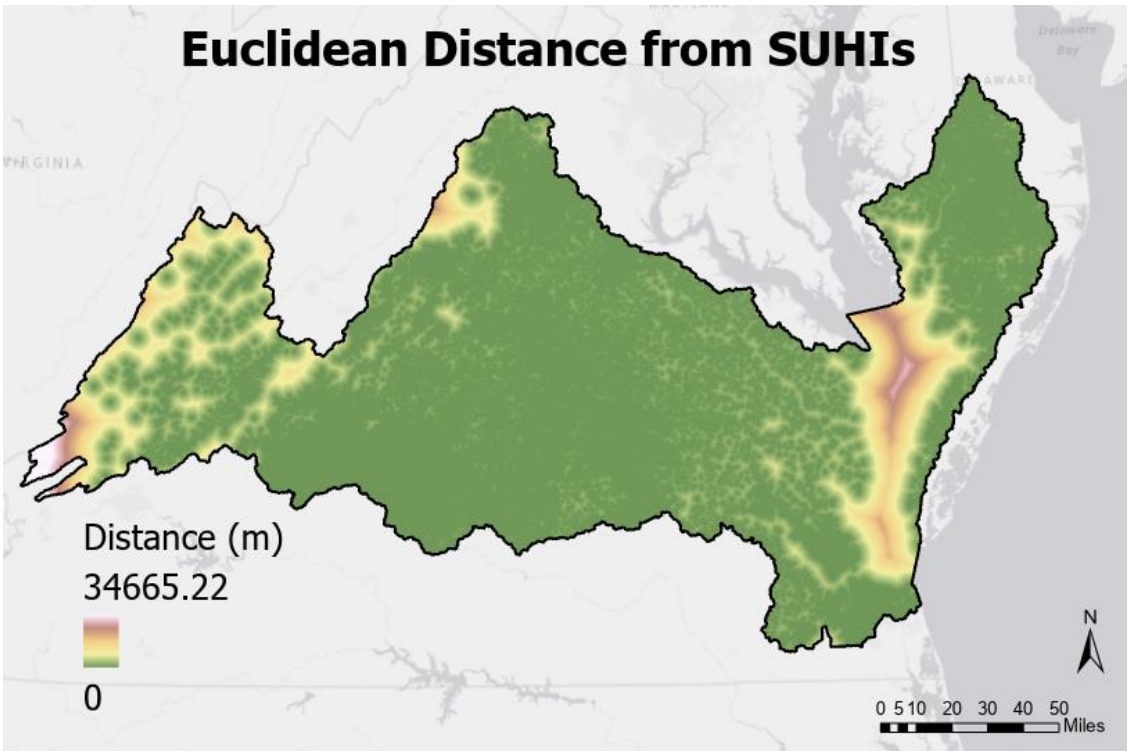

Figure 23: This map shows the distance from a pixel to the nearest SUHI for all of the areas in the study area. If the location is within a SUHI, it is on the green side of the color scheme in the legend with a distance of 0 meters.

The second approach, the omni-directional distance, between water temperatures and SUHIs is to do what was listed above as a pre-step to the first method (distance-zero) (Figure 24). The Euclidean distance tool is used to get a raster surface of the distance away from SUHIs. The value is extracted to the water temperatures points through the extract multi values to points tool which gives the distance in meters how far a water temperature point is from its nearest SUHI.

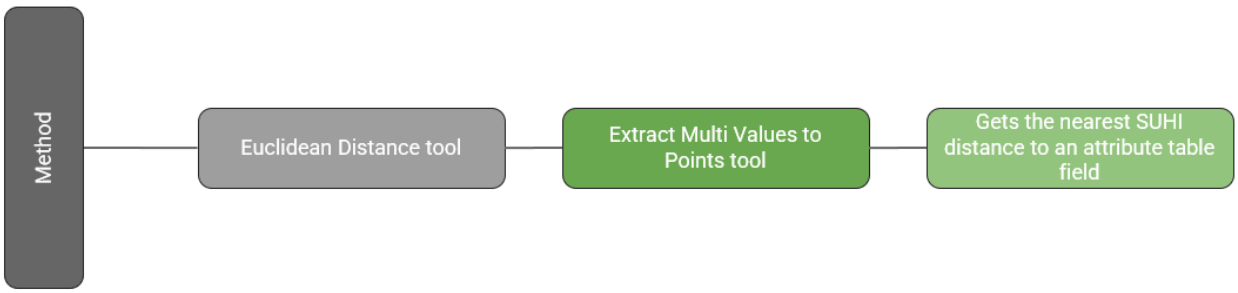

Figure 24: This flowchart shows the second distance approach's workflow of finding the nearest SUHI to a water temperature point with the omni-directional distance approach.

For the third approach, the more complex upstream/downstream distance approach, where the nearest SUHI distance that is upstream from a water temperature point is calculated, three methods are attempted. Not all of them worked. Those methods are described in the flowchart in Figure 25.

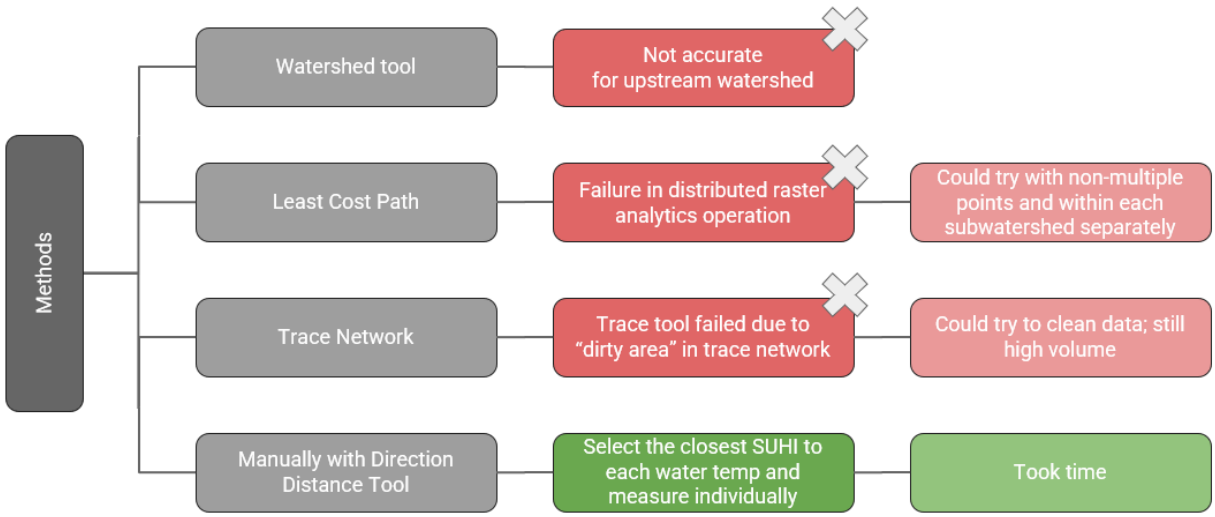

Figure 25: This flowchart shows the third distance approach's workflow of what was tried before getting to a method that worked for finding the nearest SUHI upstream from a water temperature point. The first three methods did not work, but the last one did.

The first method used the watershed tool, but this tool's output was not accurate upon inspection so it was rejected. The second method used the least cost path tool similar to the approach used by Sechu et al. (2021). This tool resulted in an error due to a failure in the distributed raster analytics operation step of the tool. While this tool could have been performed one pair of points at a time within each sub-watershed separately, this would have taken too much time, so it was rejected. For the third method, an array of tools was used to find the upstream area through a trace network, which traces the upstream stream network from a point to

find the streams flowing into that point. A smaller work area of a few sub-watersheds is used to see if the tool works at a faster pace. A trace network was created with the trace network tool, then the enable network topology tool was used, which failed when the whole study area is used. Next the trace tool was run, but it resulted in error due to too many "dirty areas" found within the trace network. The data could be cleaned in order for this tool sequence to work, but with this high volume of data it would not have been cost-effective.

The fourth method of this approach is the approach that was ultimately successful. This method required the manual calculations of the upstream distances. In practice, this consisted in looking at the water temperature locations one at a time while using the stream polylines and the slope derived from the DEM to determine which SUHIs are upstream from that location or group of points. The direction distance tool was used to find the distance in meters between the water temperature points and the nearest upstream SUHI. While this approach was time consuming, it was easy to understand to control for quality. A set of rules were developed to help determine the nearest upstream SUHIs. These are listed in the following sentences, and as discussed later in the paper can serve as a starting point for future automation of the calculation.

The first rule is that if the SUHI is upstream (having a higher stream order) from the water temperature point, then the direction distance tool is used manually. The second rule is that if the water temperature point is on land (in a stream), then use the direction distance tool on the nearest SUHI within the same sub-watershed with a higher slope. The third rule is that if the water temperature point is on water (in a wide river or the Chesapeake Bay), then use the direction distance tool on the nearest SUHI within the same sub-watershed or upstream sub-watershed if there are no SUHIs in the direct sub-watershed. The fourth rule states that if no SUHI is upstream from the water temperature point, then leave the value null. Lastly, the fifth

rule says that if the water temperature point is contained within a SUHI, then put the value at 0 meters.

3.2.4 Flowchart Steps 8 and 9

After the distances are calculated, scatter plots and box plots are created to establish the association between the water temperatures at the locations measured and its distance to the nearest SUHI location. The water temperature datapoints in degrees Celsius are on the y-axis while the distance in meters to SUHIs and other variables are on the x-axis. The scatterplots give the r-value, which is the Pearson Correlation. This is the strength of correlation between each of the two variables being compared. The closer to -1 or +1 it is, the higher the strength of association for those variables. The closer to 0 the values are, the lower the strength and the higher the randomness the correlation is. Additionally, a multiple linear regression in Excel is run to fit the pairs of variables being compared to a line and see how the dependent variable changes as the independent variable changes with the R-Squared value. An exploratory regression is also run in ArcGIS Pro to find more statistical information. Variables such as whether the data is in a stream/river or the bay, distance to shoreline, and the depth of the water for the water temperatures where it is known are regressors to see how it relates to the trend found.

The box plots are created to describe the data variables such as the distance-zero approach, categories of water temperatures, and classes of LCZs to the water temperature. The parameters displayed in the box plot are the minimum, first quartile, median, third quartile, maximum, and outliers. In addition, the water temperature averages are added to the graph to add more depth to the summary of each data variable for the water temperature.

3.2.5 Categories of Upstream/Downstream Relationships

The water temperature points are categorized into six classes depending on where the SUHIs are in relation to them within each sub-watershed. The water temperature point categories are described as: 1) contained within a SUHI; 2) SUHI upstream and downstream; 3) SUHI upstream only; 4) SUHI downstream only; 5) within a wide river with a SUHI; and, 6) No SUHI upstream and downstream or in the sub-watershed (see Figure 26). The water temperature data is categorized to assess how the average and range of the temperature increases or decreases for each case scenario.

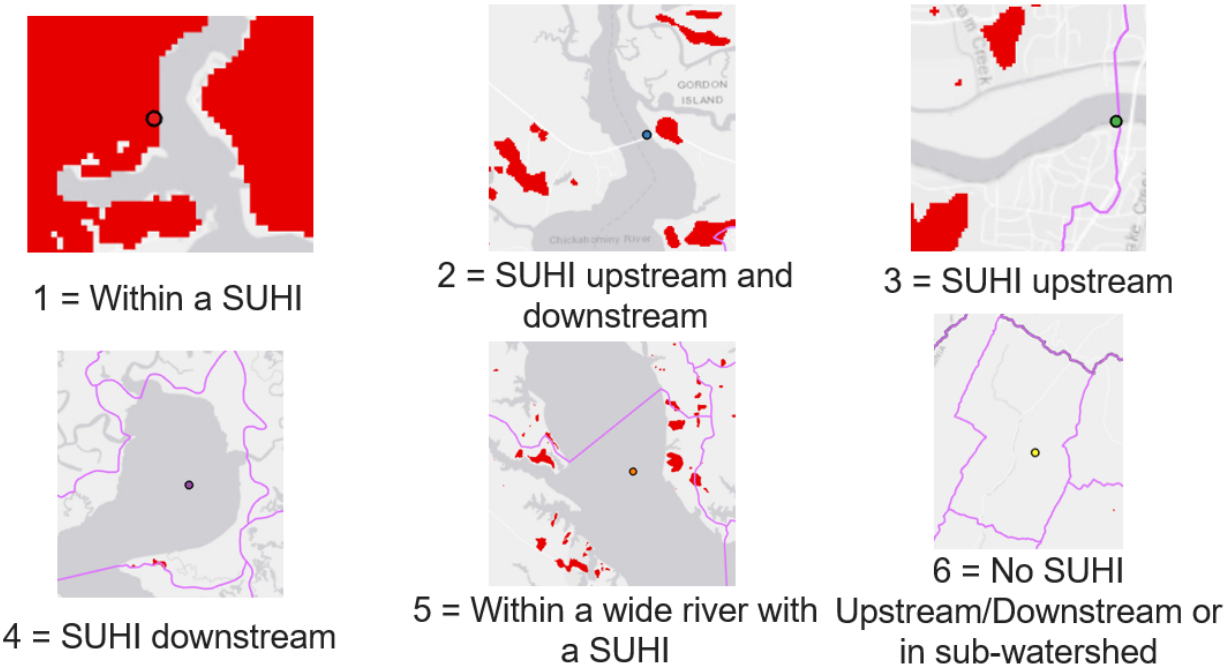

Figure 26: These images of water temperature points in different situations illustrate each of the six categories created. 1 = red, 2 = blue, 3 = green, 4 = purple, 5 = orange, and 6 = yellow.

SUHIs downstream do not have influence on the water temperatures upstream from them. So, categories 2 (SUHIs upstream and downstream) and 4 (SUHI downstream only) are combined to compare just category 3 (SUHI upstream only) to both situations that have SUHIs downstream present.

4 Results, Analysis, and Discussion

ArcGIS Pro and Microsoft Excel are used to calculate the results and evaluate the relationships between water temperature and the three different distance approaches. Box plots and scatter plots are the main form of conveying data results (see Figures 27 through 37). Additionally, the statistics retrieved from Excel's multiple linear regression and ArcGIS Pro's Exploratory Regression tool were presented. See Tables 2 through 4 for the output values of these statistical tests.

4.1 Distance Approaches Results

The box plots and scatter plots show the spread of data and trend between two different variables, respectively. A few of the boxes and points in these graphs have been symbolized by different characteristics to visualize and understand the data.

The first few graphs' results are for the distance approaches. Figure 27 below displays the first distance approach results (distance-zero or contained within SUHI). Each box plot split into two groups for the water temperature points: within a SUHI and outside a SUHI.

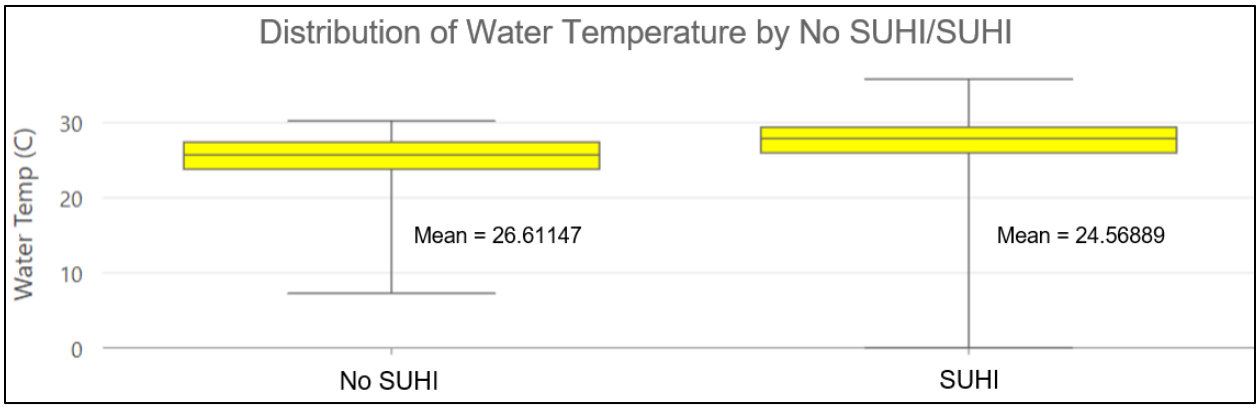

Figure 27: This box plot shows the maximum, third quantile, median, first quantile, and minimum of water temperature along with the mean in degrees Celsius for the points not within a SUHI vs. the points contained within a SUHI.

For the first distance approach that looks into water temperatures split into whether the point is within a SUHI or not, the average water temperature is higher for the group that is not within the SUHIs. That average is 26.61147 °C while the average for the water temperature points within a SUHI is 24.56889 °C, which is a little over 2 °C apart (see Figure 27 above). The regression coefficient for this relationship is -1.226597188 while the R^2 value is 0.007788809 and the r-value is -0.088254231. The coefficient and r-value have the same negative sign when the R^2 is positive; they all show a weak relationship with the low coefficient and close-to-zero values due to the categories not portraying a pattern with the water temperature. This does not follow what is expected with the hypothesis. However, the range of water temperature is longer for the group that is contained within SUHIs, which shows that there are some higher water temperatures when inside SUHIs.

Figure 28 below shows the scatter plot for the second distance approach between the water temperatures and their nearest SUHI omni-directionally.

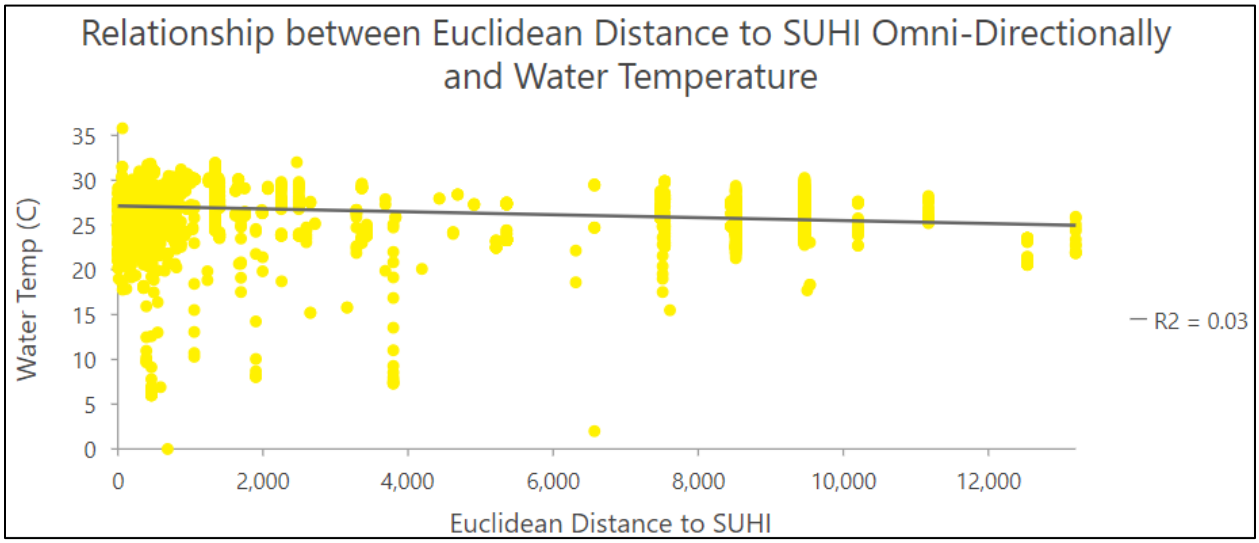

Figure 28: This scatter plot shows the linear relationship between water temperature in degrees Celsius to the nearest omni-directional SUHI in meters.

The second distance approach finds the distance to the nearest SUHI omni-directionally in meters. There is a majority of the data points clustered in the distances lower than 2,000 meters. The scatter plot that displays this relationship has a R-Squared value of 0.03, which means the line of best fit had very little connection between the two variables; only 3% of the variation was explained. The regression analysis output an R^2 value of 0.016239136, which rounds up to 0.02 and is close to the 0.03 listed in the scatter plot. The regression coefficient is -0.000206547 and the r-value is -0.127432868; both the coefficient and r-value show a negative weak relationship which is explained by the slightly negative slope of the scatter plot in Figure 28. This approach takes into account the nearest SUHI whether it may be upstream or downstream; the downstream waterways do not directly influence a water temperature point that is upstream from it, so the mixed results are expected.

Figure 29 presents the scatter plot for the third distance approach between the water temperatures and their nearest SUHI upstream from that point symbolized by classes of depth for the known water temperature depths.

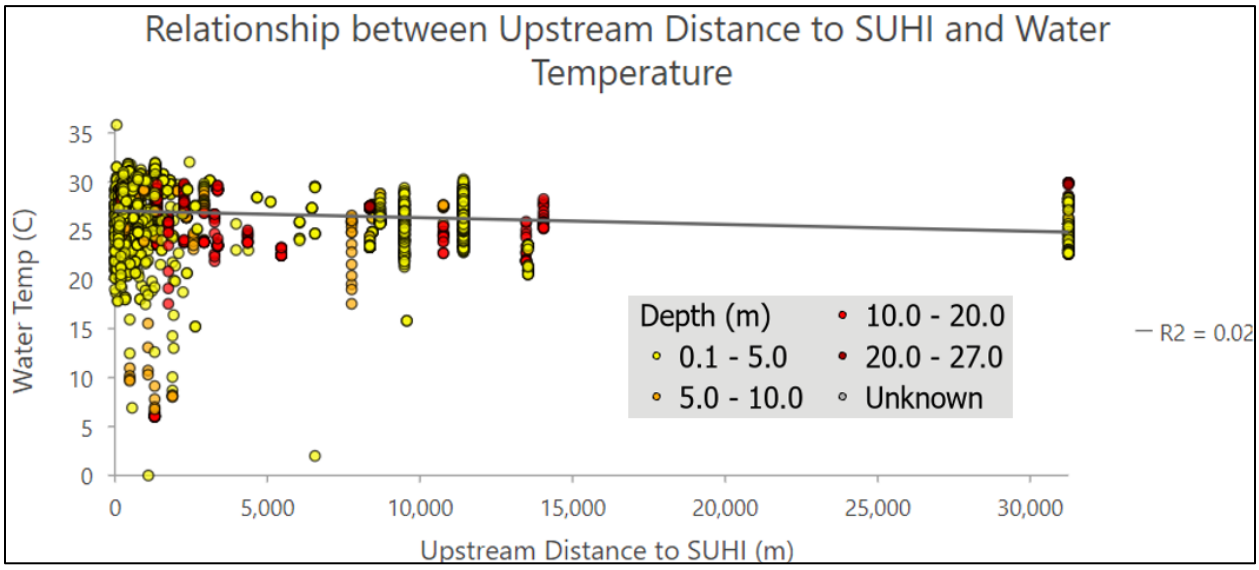

Figure 29: This scatter plot is the same as Figure 28 above, but it is symbolized and classified by the depth of the water temperature that was taken.

For the third distance approach, the water temperature is compared to its nearest upstream SUHI distance in meters and has a cluster of data in the distances lower than 5,000 meters. The R^2 value of the scatter plot is 0.02 while the regression's R^2 is 0.02292 that rounds to 0.02 as well, which means the correlation between the two variables had very little connection or variation shared. The regression's coefficient is -0.00006892 while the r-value is -0.019534627; both are negative and weak due to the relationship between water temperature and the upstream distance to SUHIs being slightly sloped downward with warmer temperatures being closer to SUHIs.

However, for both the second and third distance approaches, the scatter plots showed a slightly negative slope in the trendline, which minutely supports the hypothesis where the warmer temperatures are closer in distance. A majority of the water temperatures clustered are where the depths are shallow while the deeper water temperatures are farther away from the SUHIs. This may be due to the Chesapeake Bay being deeper and farther away from land.

4.2 Upstream/Downstream Category Analysis Results

The water temperatures are categorized into 6 categories, then further combined to make 5 categories (category 2 went into category 4). The distribution of the water temperatures within these categories were displayed in boxplots (see Figure 30 and Figure 31 below). Figure 32 is the same 5 categories from Figure 31 but split into two groups based on whether the water temperature point was in a stream/river or the bay. The following paragraphs discuss these categorizations.

The water temperature categories are listed as the water temperatures being 1) contained within a SUHI, 2) SUHI upstream and downstream, 3) SUHI upstream only, 4) SUHI downstream only, 5) within a wide river with a SUHI, and 6) No SUHI upstream and downstream or in the sub-watershed. When looking at the box plot of the six categories (see Figure 30), the lowest water temperature average is 24.70234 °C when the point is contained within a SUHI. This is an unexpected result because it is the opposite of what the hypothesis claimed; this does not support the hypothesis. The rank of the averages from least to greatest by category is 1, 3, 6, 2, 4, and 5.

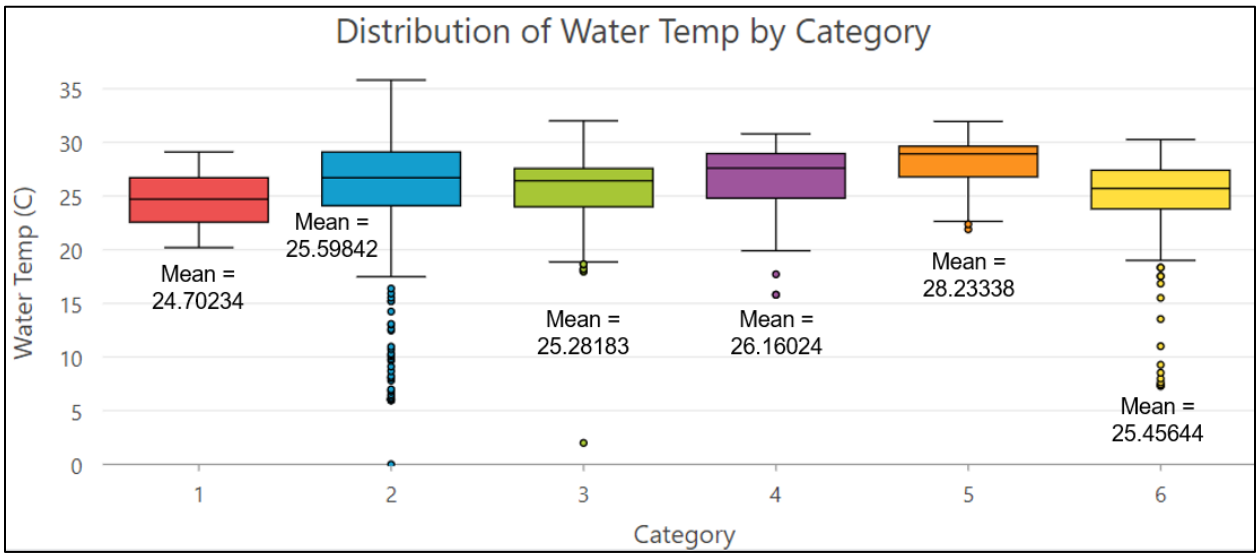

Figure 30: This box plot shows the maximum, third quantile, median, first quantile, and minimum of the water temperatures along with the mean in degrees Celsius for each category 1 through 6.

The water temperature categories are re-evaluated and category 2 is combined into category 4 to make a total of five categories. This is done to group the categories that contain SUHIs downstream from a water temperature point. Figure 31 shows the box plots for these five categories; the only mean that changes is category 2 & 4 which are one category. Its new average

is 25.63874 °C which is lower than what it was before because category 2 brings it down. The new ranking of categories from least to greatest is 1, 3, 6, 2 & 4, and 5, which does not change the order.

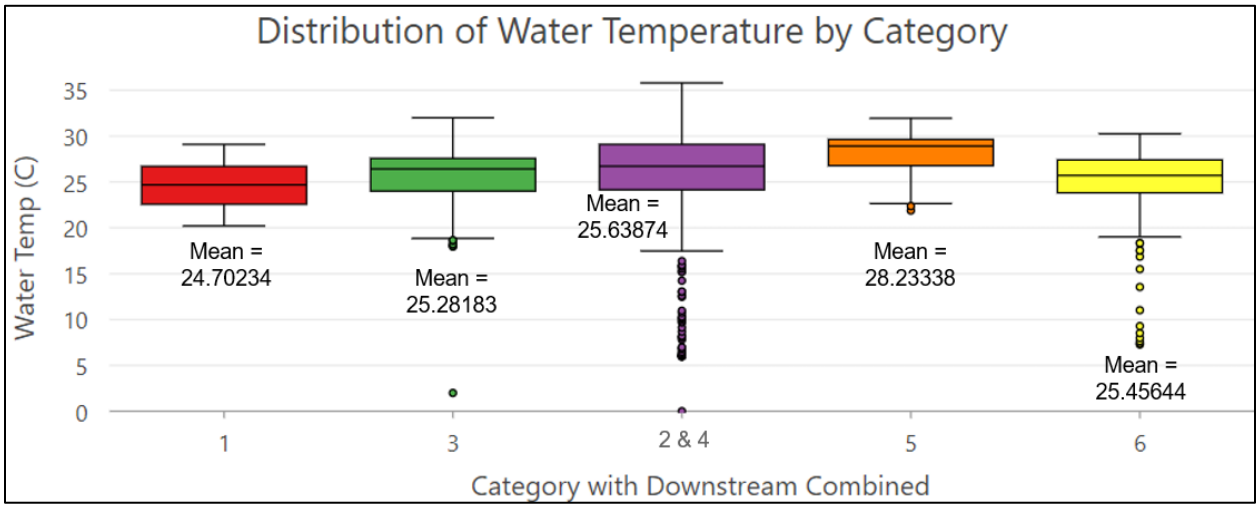

Figure 31: This box plot shows the maximum, third quantile, median, first quantile, and minimum of water temperatures in degrees Celsius for categories 1, 3, 2 & 4, 5, and 6. Notice the blue category 2 data is combined into the purple category 4 class.

Furthermore, Figure 32 splits the data and categories in Figure 31 by the body of water it inhabits; the two groups are stream/river and bay. Category 1 does not have any water temperature points within the Chesapeake Bay because SUHIs are only on land; therefore, there is not an average or box plot for the bay in that category. Categories 3 through 5 have a higher water temperature average in the streams/rivers group than the bay group. This shows that the shallower waters are warmer when they contain a SUHI somewhere in the sub-watershed. Category 6 has the higher water temperature average within the bay group instead of the stream/river group; this means that there is a lower water temperature average for the streams and rivers that do not have a SUHI in their sub-watershed. This supports the hypothesis of this paper. One potential reason why the data spread out the way it did is that the majority of the

water temperature data points fall under category 2 & 4. The other categories do not have as many data points to have as much of a solid outcome as category 2 & 4.

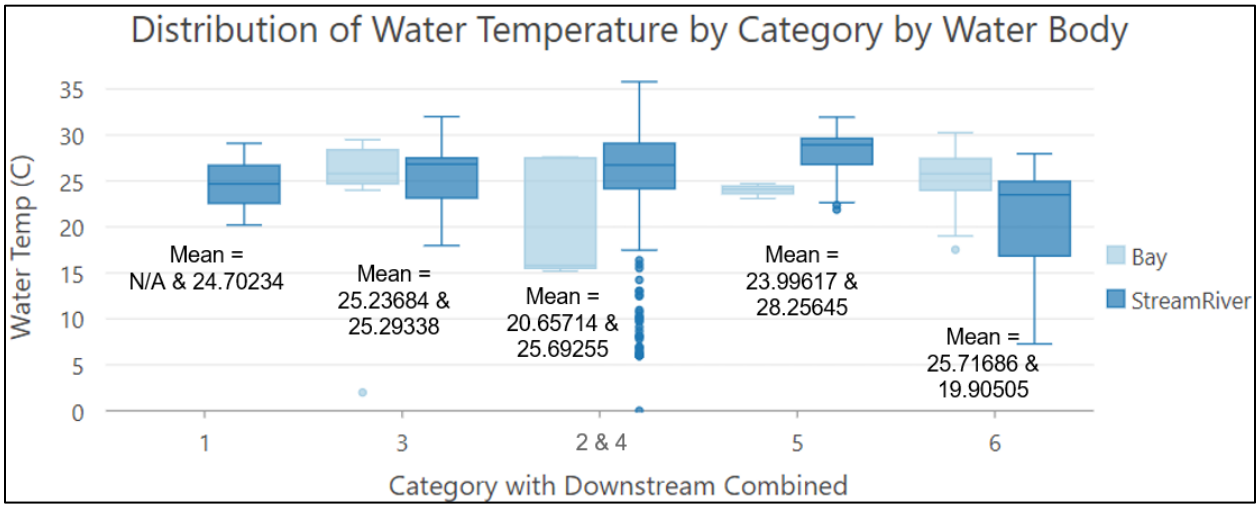

Figure 32: This box plot shows the maximum, third quantile, median, first quantile, and minimum of water temperature in degrees Celsius for categories 1, 3, 2 & 4, 5, and 6 split into two groups. The groups are if the water temperature point is in a stream or river or in the Chesapeake Bay.

4.3 Other Variables

The four following scatter plots in Figures 33-36 show the relationship between water temperature and elevation, distance to the shore, NDVI, and NDBI, respectively. They are color coded by the 5 categories of water temperature situations. The following paragraphs discuss the scatter plots.

The scatter plot for the correlation between water temperature and elevation has an R-Squared value of 0.12 in the scatter plot and 0.174916568 in the regression, so it is more connected than the other scatter plots (see Figure 33). If the elevation is higher, then the water temperature is cooler (Choi et al. 2014). The regression's coefficient is -0.013535057 while the r-value is -0.418230281. They are both negative because the slope goes downwards (because

higher elevations have cooler temperatures), but the r-value shows a moderately strong trend due to it being almost halfway to -1.0.

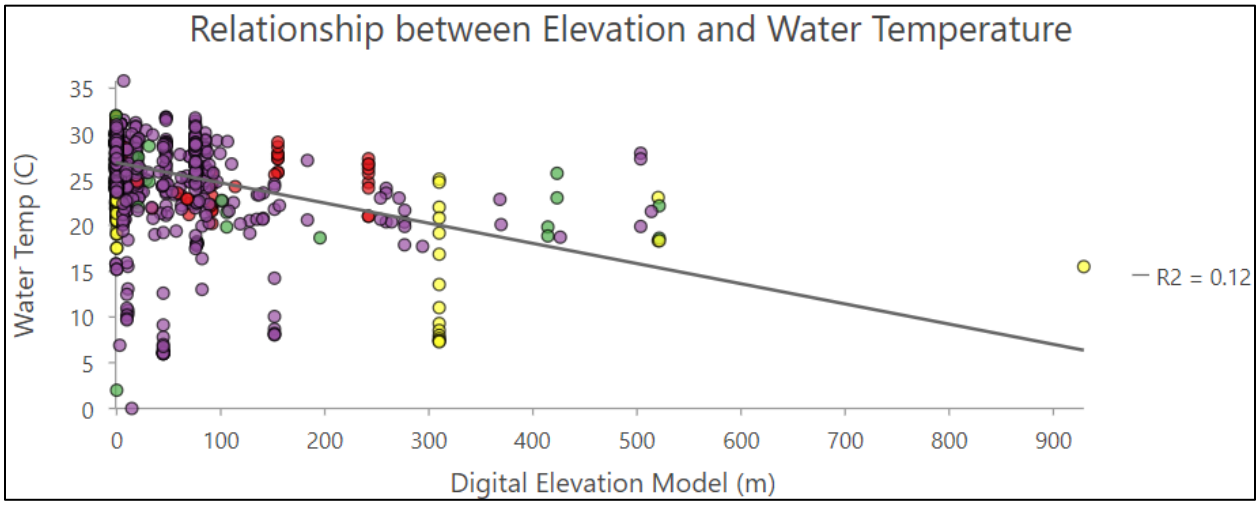

Figure 33: This scatter plot shows a stronger relationship with a steeper slope between the water temperatures in degrees Celsius and elevation in meters. The colored classifications match the different water temperature point categories 1 (red), 3 (green), 2 & 4 (purple), 5 (orange), and 6 (yellow).

In the beginning of the paper, the water temperature points were sized proportionally and color-coded in Figure 5. There was a clear pattern that the warmer water temperatures were near the shoreline; Dihkan et al. (2015) mention that coastal cities are more vulnerable to SUHI impacts. Figure 34 displays the trend between water temperatures and their distance to the shore.

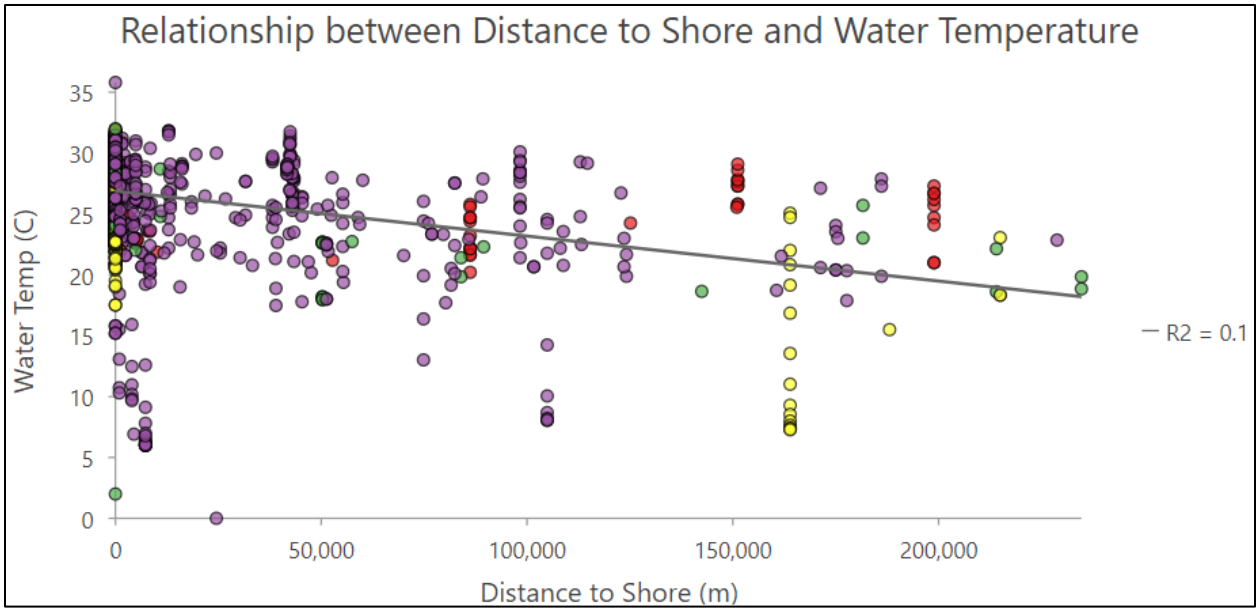

Figure 34: This scatter plot shows the water temperature in degrees Celsius compared to its distance to the shoreline of the Chesapeake Bay in meters. The colored classifications match the different water temperature point categories 1 (red), 3 (green), 2 & 4 (purple), 5 (orange), and 6 (yellow).

The scatter plot for the relationship between water temperatures and their distance to shore had an R-Squared value of 0.10 while the regression's value had a value of 0.16480232, so the line of best fit is almost as varied as the water temperature and elevation model. There is 10%, or 16% with the regression, variation between these two data variables. The regression's coefficient is -1.8701E-05, which is very small while the Pearson's r-value is -0.40595852. Similar to the water temperature and elevation relationship, the water temperature and distance to shore relationship is moderately strong with its r-value and the r-value and coefficient are both negative like the slope of the line of best fit.

The water temperature vs. NDVI relationship showed a slightly negative slope with an R-Squared value at 0.11 in the scatter plot and 0.1079 that rounds to 0.11 in the regression analysis, which means there is little connection between the two variables but NDVI's line of best fit is one of the higher ones. The regression coefficient is -10.72394 while the r-value is -0.427231349

both are negative due to the slope and strong due to the high coefficient and moderate r-value. The NDVI values are higher where the water temperatures are cooler; the vegetation is healthier and greener when the values are high (see Figure 35). NDVI is the third strongest variable in relation to water temperature.

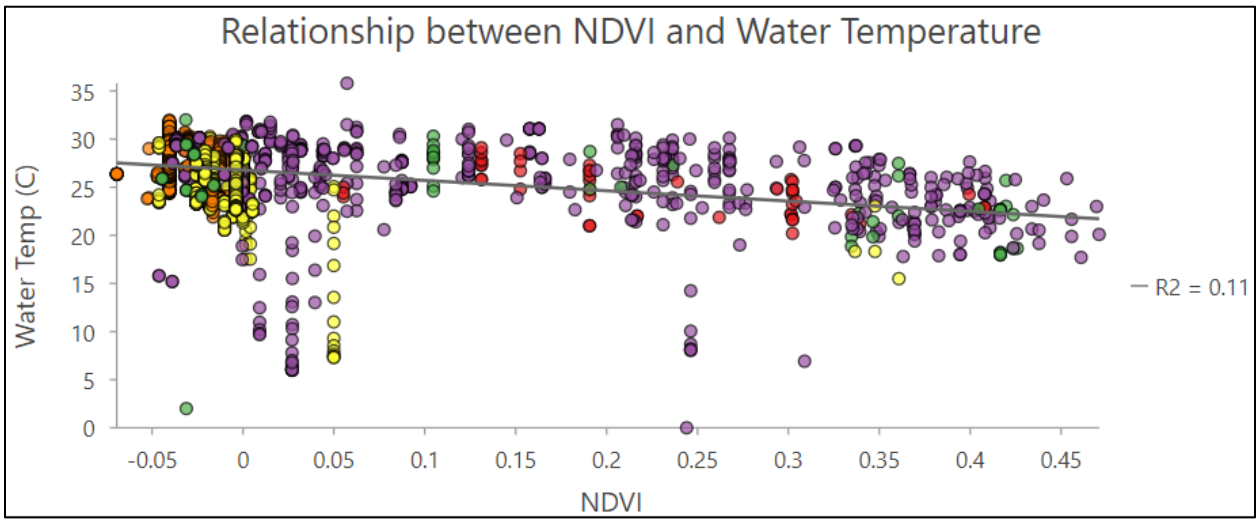

Figure 35: This scatter plot shows the water temperature in degrees Celsius compared to that point's normalized difference vegetation index value. The colored classifications match the different water temperature point categories 1 (red), 3 (green), 2 & 4 (purple), 5 (orange), and 6 (yellow).

The opposite pattern is seen for NDBI because instead of greenery being a higher value, it is a lower value. Macarof and Statescu (2017) stated that "NDBI is an accurate indicator of surface UHI effects and can be used as a complementary metric to the traditionally applied NDVI." When the NDBI value is higher, more built-up and urban, the water temperatures are warmer (see Figure 36). This is expected and supports the hypothesis that the water temperatures are warmer when you get closer to SUHIs, which consist of built-up land covers. These findings with NDVI and NDBI relate to what Kaplan et al. (2018) concluded in their study.

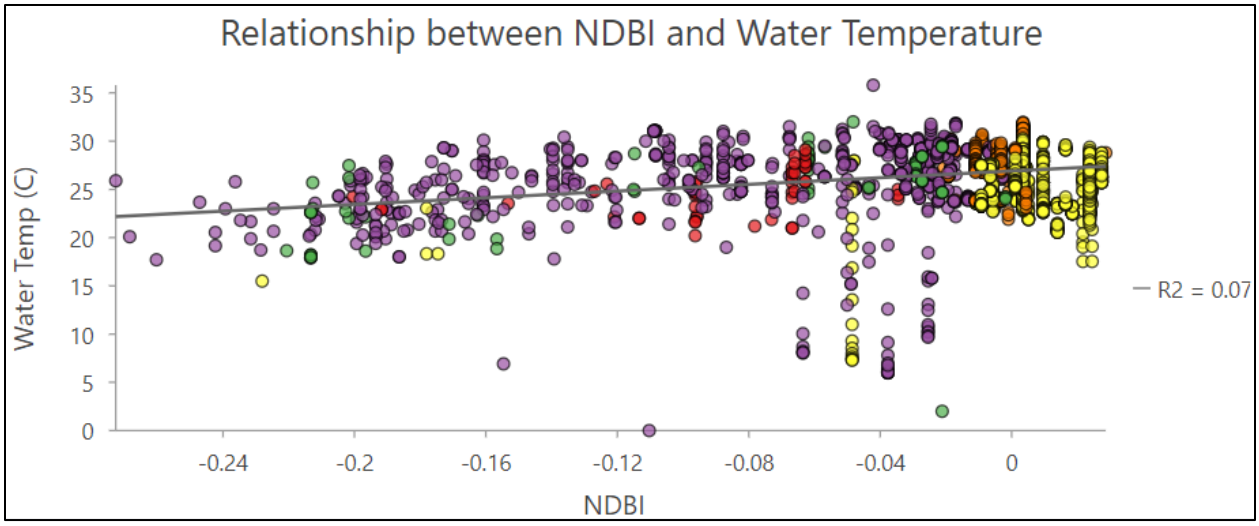

Figure 36: This scatter plot shows the water temperature in degrees Celsius compared to that point's normalized difference build-up index value. The colored classifications match the different water temperature point categories 1 (red), 3 (green), 2 & 4 (purple), 5 (orange), and 6 (yellow).

The water temperature and NDBI scatter plot has an R^2 value of 0.07, which is what the regression's value is rounded up from 0.06551. The regression coefficient is 17.31023 and the r-value is 0.388414478; these values are both positive because the slope of the line of best fit is positive this time and the relationship is direct. The coefficient is high while the r-value is moderately strong, so this relationship is strong although it is on the other end of the spectrum with a positive relationship.

4.4 Local Climate Zones Results

The final graphic result is the box plot that shows the water temperature distribution and averages for each LCZ land class that is within the study area. LCZs describe the climate zone of a local area. Figure 37 shows the water temperature by LCZ classes; the study area only includes 9 of the 17 land classes. The ranking of LCZ water temperature averages going from least to

greatest are 11 (dense trees), 12 (scattered trees), 9 (sparsely built), 8 (large lowrise), 6 (open lowrise), 10 (heavy industry), 17 (water), 5 (open midrise), and 14 (low plants).

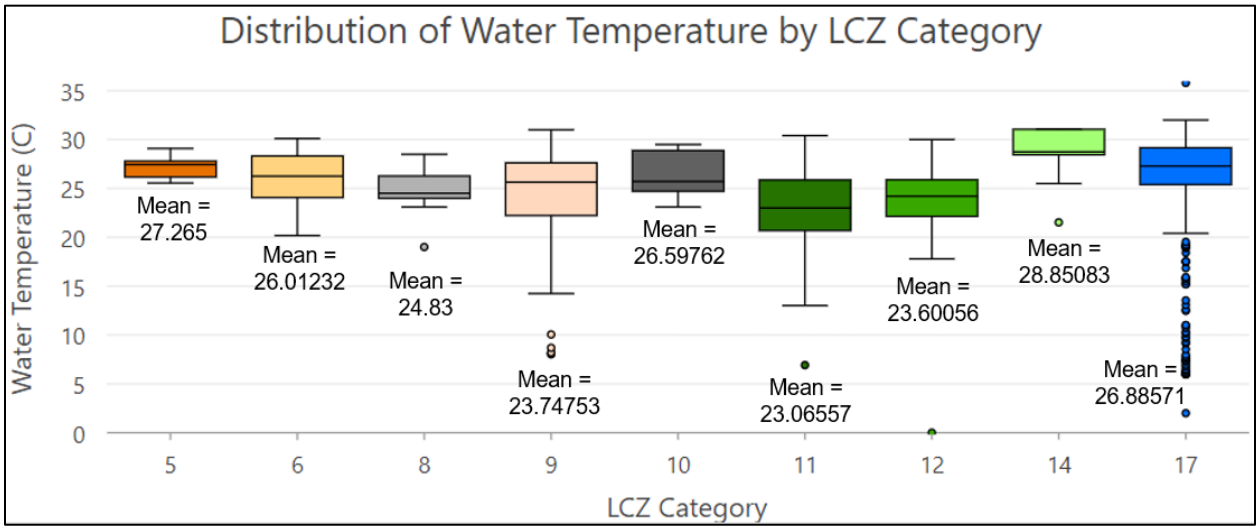

Figure 37: This box plot shows the different local climate zones within the study area and their maximum, third quantile, median, first quantile, and minimum of water temperature in degrees Celsius. The LCZ land classes are 5 = Open Midrise, 6 = Open Lowrise, 8 = Larger Lowrise, 9 = Sparsely Built, 10 = Heavy Industry, 11 = Dense Trees, 12 = Scattered Trees, 14 = Low Plants, and 17 = Water.

The ranking output of the LCZs is expected with the exception of the highest water temperature average being within the low plants land class, which is unexpected to some degree. Vegetative land covers like forest cool down an area due to the cooling effect of shade that the trees bring, but low plants do not have as much shade hence why it is warmer. What is surprising is that the low plants have a higher water temperature average than the heavy industry land class. There may not be enough water temperature points within each LCZ land class, so this could be a potential cause of the unexpected results that limit the pattern of water temperature average.

4.5 Pearson Correlation and Multiple Linear Regression Results

The Pearson Correlation test was calculated in Excel with the =PEARSON function to gather the r-values for the selected variables in Table 2. The strongest, least random variables are NDVI, elevation, distance to shore, and NDBI with r-values of -0.427, -0.418, -0.406 and 0.388, respectively. These values mean that the corresponding variables are moderately strong. NDVI, elevation, and distance to shore have a negation relationship (inverse) while NDBI has a positive relationship (direct). The other confounding factors such as distance to urban land cover and depth are positive, random correlations with water temperature. The depth data was incomplete so this may be why the r-value is closer to zero.

Water Temperature vs.	Pearson Correlation r-Value
NDBI	0.388414478
Depth	0.139004198
Distance to Urban NLCD	0.033191568
Distance to Upstream SUHI	-0.019534627
Not Within SUHI/Within SUHI	-0.088254231
Euclidean Distance to SUHI	-0.127432868
Distance to Shore	-0.40595852
Elevation	-0.418230281
NDVI	-0.427231349

Table 2: Excel's Pearson Correlation test output ranked from most positive to zero to most negative (blue to white to red)

The multiple linear regression results from Excel are in Table 3. The variables that were run are listed under the variable column. The R-Squared, coefficients, standard error, and P-value are the parameters selected from the output to display in the table. Also, the exploratory regression results from ArcGIS Pro are in Table 4. The percentage of significance and the overall Adjusted R-Squared, which is more unbiased and better to use than the normal R-Squared, is listed for the 9 variables that are included.

Regression Statistics				
Variable	R Square	Coefficients	Standard Error	P-value
Not Within SUHI/Within SUHI	0.007788809	-1.226597188	0.882675222	0.165896
Euclidean Distance to SUHI	0.016239136	-0.000206547	0.000102498	0.044978
Distance to Upstream SUHI	0.02292	-0.00006892	8.46E-06	5.44E-16
Distance to Shore	0.16480232	-1.8701E-05	2.68418E-06	2.95E-11
Distance to Urban NLCD	0.00110168	7.43993E-05	0.000142835	0.602921
Elevation	0.174916568	-0.013535057	0.001874243	6.4E-12
NDBI	0.06551	17.31023	1.23443	2.20E-16
NDVI	0.1079	-10.72394	0.5828	2.20E-16
Depth	0.0002148	-0.01827	0.1666	0.273

Table 3: Excel's multiple linear regression output.

For the multiple linear regressions run in Excel, all of the variables that underwent the process had R-Squared values that were small. The three variables that had a stronger connection and variation compared to the rest were elevation, distance to shore, and NDVI. Their R-Squared values were 0.174916568, 0.16480232, and 0.1079, respectively, while depth, distance to urban land cover, not within SUHI/within SUHI, Euclidean distance to SUHI, distance to upstream SUHI, and NDBI had values around 0.0002-0.02 going from least to greatest. These low values show that these confounding factors that were looked at in this study are randomly related to water temperature.

For the exploratory regression run in ArcGIS Pro, the summary of the variables' significance is calculated. The variables that had 100.00% significance are elevation, Euclidean distance to SUHI, and NDVI with upstream distance to SUHI coming in close at 99.22%. The lowest significance was with the within SUHI/not within SUHI variable at 30.86% because that variable was a category and did not show a strong r-value. Flow accumulation was another confounding factor looked at in this regression; it ended up with a significance of 81.25%, which is high. Table 4 lists the significance mentioned for the selected variables. The overall Adjusted

R-Squared was 0.23 which is the highest line of best fit seen in this study. However, values over 0.50 have more variation shared between the variables.

Summary of Variable Significance			
Variable	% Significant	% Negative	% Positive
Elevation	100.00	100.00	0.00
Euclidean Distance to SUHI	100.00	100.00	0.00
NDVI	100.00	100.00	0.00
Upstream Distance to SUHI	99.22	100.00	0.00
Distance to Nearest Urban NLCD	92.19	50.00	50.00
NDBI	88.28	50.00	50.00
Flow Accumulation	81.25	96.88	3.12
Distance to Nearest Shore	62.89	51.17	48.83
Within SUHI/Not Within SUHI	30.86	80.86	19.14
Overall Adjusted R-Squared: 0.23			

Table 4: ArcGIS Pro's exploratory regression output.

4.6 Discussion

The hypothesis for this paper is that the closer a water temperature point is to a SUHI, the warmer the water temperature is. Three distance approaches are developed to explore different pathways to establish this relationship. Their results are discussed further in the following sections along with the other variables that supplement them.

4.6.1 Distance Approaches Discussion

The distance relationships explored show that when a water temperature point is within a SUHI, the water temperature is cooler than with the SUHI upstream of the point. A possible explanation for this distance pattern is that there is a spatial lag to the SUHI's influence on water temperatures; this is a theory proposed by me. Two pieces of literature that use a similar theory are Arrigoni et al. (2008) with lagged water temperature and Wrzesiński and Graf (2022) with allochthonicity. This means that the area downstream the SUHIs are influenced by the SUHIs

more than when it is directly within the SUHI (Cuba et al. 2019). It takes a distance or certain amount of water for the warmer water temperature to fully flow and influence the water temperature point downstream from the SUHI. Furthermore, the cooler water temperatures upstream from a SUHI flow into the SUHI's water temperature points which may make it a lower temperature. Groundwater flows into streams as well and is another confounding factor to take into account (Arrigoni et al. 2008). Kaplan et al. (2018) find that UHIs within their study area were found in many suburban areas; this supports the spatial lag theory since sub-urban areas are outside of heavily developed urban centers.

A difficulty was encountered when calculating the nearest upstream SUHI distances. The method was done manually, so this Capstone study benefits from an automation of code that can find and measure the nearest upstream SUHI efficiently.

4.6.2 Category Discussion

The water temperature categories to elaborate further are 5 and 6. Category 5 is the water temperatures within wide rivers. It is a separate category because they have streams flowing into them and more than one sub-watershed influences that point. This category has the highest average water temperature at 28.23338 ℃, which is not too surprising since all the streams going through SUHIs upstream flow to that point. Category 6 is the water temperature points that don't have a SUHI upstream and downstream or in the sub-watershed, so this is expected to be the coolest temperature. But it is the third least water temperature average, which is a surprising result. This may be higher ranked because it mainly includes the water temperatures points within the Chesapeake Bay. The bay has all the streams and rivers flowing into it and mixing the deep and tidal waters while evaporating is occurring, so numerous water temperatures are influencing that one point.

4.6.3 Other Variables Discussion

Many variables are explored in this study such as elevation, NDVI, NDBI, NLCD, depth at some points, flow direction, and flow accumulation. One major limitation with the collected datasets was that not all of the water stations had depth data with their measurements. Other factors to take into account include wind speed and solar radiation as mentioned in Yang et al. (2020), weather events that affect satellite imagery, dissolved oxygen content like explored in Harvey et al. (2011), and biota influences like algae blooms. Additionally, there are anthropogenic factors that are stressors, which include "increased watershed imperviousness, destruction of the riparian vegetation, increased siltation, and changes in climate" (Nelson and Palmer 2007).

The scatter plot for the correlation between water temperature and elevation illustrates that the higher the elevation is, the cooler the water temperature is. This is understandable and expected because there are typically cooler temperatures at higher altitudes like Shenandoah National Park and its mountain range. Bechtel et al. (2019) mention topography as having an influence on the SUHIs. The NDVI values are higher while the NDBI values are lower where the water temperatures are cooler (see Figures 35 and 36). This was an expected result, which supports the hypothesis that the cities, where there are SUHIs, are where warmer water temperatures are located.

The other confounding factors not investigated in this study that play a role in SUHI development are important to consider to get the whole picture and to control for all influences on the environment that deal with the study. Wind speed is a factor because wind can cool down an area with evaporation/evapotranspiration or move the heat elsewhere. The LST data is from Landsat satellite imagery and if there are weather events like droughts, extreme heat, and heavy

precipitation, they have an effect on the values shown in the remote sensing bands. For example, thermal band 10 which is turned into the LST map in Figure 9 has areas where it is darker and cooler (the second bump of the study are in the north and on the western tip) or brighter and warmer (the southwestern portion of the study area). The darker, cooler areas may be due to heavy precipitation and the brighter, warmer areas may be due to drought. The southwestern portion of the study area that is brighter and warmer (red in Figure 9) is the agricultural fields outside of Lynchburg. This SUHI output was not expected and is a limitation to understanding the relationships explored.

Next, the dissolved oxygen content within water influences its temperature. If the dissolved oxygen is high, then the assumption is that oxygen is being introduced from the atmosphere because the water is flowing fast, and so the water is cooler. In comparison, if the dissolved oxygen is lower, then the water is warmer. Algae blooms affect the amount of dissolved oxygen in a body of water; the more algae there is, the more decomposition and decreased dissolved oxygen content. Algae blooms circulate in a positive feedback loop, which means that it gets worse and accumulates as time goes on. It is important to take into account all of the different factors to see the true outcome of the water temperature vs. proximity to SUHI relationship.

4.6.4 Local Climate Zones Discussion

Demuzere et al.'s (2022) global map was used to obtain the LCZs for the study area, but there is a more accurate way of defining these LCZs. Demuzere et al. (2021) have a methodology that creates the LCZs and is what created the global map of LCZs. However, it would have been better to carry out this methodology for only the study area in order for it to be portrayed to the best of the method's abilities. Demuzere et al.'s (2021) methodology uses training areas created by the user for each LCZ which becomes the input for their LCZ Generator tool. Bechtel et al.

(2019) finds that using LCZs with SUHIs is strongly recommended due to the significant LST differences found between built-up and natural land classes.

Due to time constraints, this study did not create the training areas to be specific to the study area and instead used Demuzere et al.'s 2022 version of the global map of LCZs. The LCZs are used to validate the SUHIs identified in this study using the overlap between the two variables. Given more time, this study could show stronger distance relationships seen in the graphs if only the validated SUHIs were used to make the water temperature and distance relationship correlations. The relationships and analysis presented in this paper may have been impacted by the decision to use the SUHIs including the non-LCZ validated areas.

4.6.5 Pearson Correlation and Multiple Linear Regression Discussion

The three variables that had a stronger connection and variation compared to the rest were elevation, distance to shore, and NDVI. The P-values are significant for the Euclidean distance to SUHI, distance to Shore, distance to urban NLCD, and elevation (DEM) due to the value being under 0.05. The values that are not significant are the first distance approach's no SUHI/SUHI zero-distance, distance to urban land cover, and depth. The first distance approach hadn't supported the hypothesis at all, so its insignificance is not surprising. The depth data was not available for all water temperature points, so only certain measurements are represented, so insignificance is not surprising for that variable either. The other variables that have significance percentages above 50% from greatest to least are distance to nearest urban NLCD, NDBI, FA, and distance to nearest shore. The last one is the no SUHI/SUHI zero-distance approach with a significance percentage of 30.86%. The overall Adjusted R-Squared is 0.23, which is the strongest correlation found within the data; it takes into account many variables to explain the outcome. Furthermore, both Excel's multiple linear regression and ArcGIS Pro's exploratory

regression found the same results that elevation is an important factor in water temperatures while the first distance approach's results are not significant.

4.7 Future Work

There is room for future work in this research study given more time. To make this data better, it would be good to have many summers averaged together for the Landsat tiles and water temperature points. The data should come from July and August and not include the month of June due to its cooler temperatures; the summer season does not start until late June. This enables more data to be collected for the higher elevations in the study area. Additionally, calculating the variables such as LST, NDVI, and NDBI individually per Landsat tile would make the tiles blend better. The depth data has many null values from the NWQMC source where the water temperature datapoints are derived. It would be an improvement if data was found with all the sources having depth measurements. The depth is an important influencer on water temperature data because if it is taken at a shallow depth, then the temperature may be warmer due to it having increased exposure to the sun's rays and less density. Knowing the total depth to the bottom of a body of water also helps because elevation data does not cover bodies of water such as the Chesapeake Bay and bathymetric data was not found for this study. All the factors that influence SUHIs and water temperatures need to be covered so that it takes into account the environment and sets controls in order to see a real pattern in the data. A major limitation in this research was the datasets available.

In the future, with more time, it is recommended to create training areas for classifying the LCZs with Demuzere et al.'s (2021) methodology. Training areas created by the researcher for only the study area is better than using the global map of LCZs that are generalized. Furthermore, using the urban LCZ validated SUHIs with the methodology and analysis would be

an improvement since this study only identifies them instead of using them. Another distance approach that was not finished may have showed a different relationship between water temperatures; this approach was calculating the upstream acreage of SUHIs that accumulate and influence the corresponding water temperature point. There may be other distance approaches to explore as well as scientific literature on SUHIs and their impacts on water increase.

5 Conclusion

This study aimed to identify what the distance relationship is between water temperatures and their proximity to SUHI locations. It is found that there are land surfaces within the lower Chesapeake Bay watershed from the summer 2019 that exhibit the characteristics and measurements of surface urban heat islands. Urban centers including but not limited to Richmond, Virginia Beach, Norfolk, Fredericksburg, Newport News, Charlottesville, and Lynchburg are dense areas of SUHIs. However, the hypothesis of water temperatures being warmer when closer to SUHIs is not supported for the lower Chesapeake Bay watershed in Virginia and some areas in West Virginia, Maryland, and Delaware. There is no strong linear pattern between water temperature and the nearest SUHIs based on the r- and R-Squared values found for each distance relationship, although the variables of elevation, NDVI, and Euclidean distance to SUHIs have a strong significance to the water temperatures measured. Factors not addressed in this study's methodology need to be taken into account in the future along with using the validated SUHIs in order to get a more accurate correlation between the water temperatures and their distance to SUHIs. Additionally, the decision to use all SUHIs identified and not only the ones LCZ validated may have influenced the outcome of the relationships.

The parts of this methodology that worked were the process of identifying SUHIs and the first two distance approaches (no-SUHI/SUHI and Euclidean distance to SUHIs). These two

approaches were easier to obtain through the use of ArcGIS Pro tools. The part that didn't work the best is the last distance approach (upstream distance to SUHIs). This approach was more complex, took up a lot of time, and the workflows had to be done manually in order to get the distance data needed for the relationship. One thing I would have done differently are to use the LCZ validated SUHIs for distance analysis, but this dataset was collected after most of this study's analysis was calculated. Another would be to research data availability for confounding factors not explored in this paper such as wind within the study area. Overall, data that holds all the necessary SUHI and water temperature influencing factors and newer technology for easier tool use could make this study go more smoothly.

6 Bibliography

Arrigoni, Alicia S., Geoffrey C. Poole, Leal A. K. Mertes, Scott J. O'Daniel, William W. Woessner, Steven A. Thomas. 2008. "Buffered, lagged, or cooled? Disentangling hypoerheic influences on temperature cycles in stream channels." Water Resources Research. 44(9): 1-13. doi: 10.1029/2007WR006480

Bechtel, Benjamin, Mattias Demuzere, Gerald Mills, Wenfeng Zhan, Panagiotis Sismanidis, Christopher Small, James Voogt. 2019. "Suhi analysis using local climate zones—a comparison of 50 cities." Urban Climate 28:1–18.

Chen, Xiao-Ling, Hong-Mei Zhao, Ping-Xiang Li, and Zhi-Yong Yin. 2006. "Remote Sensing Image-Based Analysis of the Relationship between Urban Heat Island and Land Use/Cover Changes." Remote Sensing of Environment 104: 133-146. doi: 10.1016/j.rse.2005.11.016.

Choi, Youn-Young, Myoung-Seok Suh, Ki-Hong Park. 2014. "Assessment of surface urban heat islands over three megacities in East Asia using land surface temperature data retrieved from COMS." Remote Sensing 6:5852–5867.

Clinton, Nicholas, and Peng Gong. 2013. "Modis Detected Surface Urban Heat Islands and

Sinks: Global Locations and Controls." Remote Sensing of Environment 134: 294-304. doi: 10.1016/j.rse.2013.03.008.

Cuba, Nicholas, Benjamin Fash, John Rogan, Anam Khan, José-Luis Palma Herrera, Rafael Enrique Corrales Andino, Claudia Nataly Mondragón Rivera, Sara Martinez, Scott Sellwood. 2019. "Measuring and categorizing the water-related downstream risks associated with mineral extraction in Honduras: How severe, and how distributed?" Applied Geography. 111:1–10.

Demuzere, Mattias, Jonas Kittner, Benjamin Bechtel. 2021. "LCZ generator: A web application to create local climate zone maps." Frontiers in Environmental Science 9:1–18.

Demuzere, Mattias, Jonas Kittner, Alberto Martilli, Gerald Mills, Christian Moede, Iain D. Stewart, Jasper van Vliet, Benjamin Bechtel. 2022. "Global map of local climate zones." Zenodo. November 15. https://zenodo.org/record/7324909

Dihkan, Mustafa, Fevzi Karsli, Abdulaziz Guneroglu, Nilgun Guneroglu. 2015. "Evaluation of surface urban heat island (suhi) effect on coastal zone: The case of istanbul megacity." Ocean & Coastal Management 118:309–316.

EPA. 2022a. "Heat Island Cooling Strategies." EPA. Environmental Protection Agency. September 16. https://www.epa.gov/heatislands/heat-island-cooling-strategies

EPA. 2022b. "Heat Island Impacts." EPA. Environmental Protection Agency. September 2. https://www.epa.gov/heatislands/heat-island-impacts

EPA. 2022c. "Learn About Heat Islands." EPA. Environmental Protection Agency. September 2. https://www.epa.gov/heatislands/learn-about-heat-islands.

Grothe, Pamela, and Adam Lynch. 2022. "Commentary: Urban Heat Islands Make Climate Change Worse." Fredericksburg.com. The Free Lance-Star. August 20. https://fredericksburg.com/opinion/columnists/commentary-urban-heat-islands-make-climate-change-worse/article_9567801c-ea7a-5ec6-a422-40e4f21954e3.html.

Haashemi, Sirous, Qihao Weng, Ali Darvishi, Seyed Kazem Alavipanah. 2016. “Seasonal variations of the surface urban heat island in a semi-arid city.” Remote Sensing 8:1–17.

Harvey, Richard, Leonard Lye, Ali Khan, and Renee Paterson. 2011. “The Influence of Air Temperature on Water Temperature and the Concentration of Dissolved Oxygen in Newfoundland Rivers.” Canadian Water Resources Journal 36(2): 171-192. doi: 10.4296/cwrj3602849.

Huang, Ganlin, M. L. Cadenasso. 2016. “People, landscape, and Urban Heat Island: Dynamics among neighborhood social conditions, land cover and surface temperatures.” Landscape Ecology 31:2507–2515.

Kaplan, Gordana, Ugur Avdan, and Zehra Yigit Avdan. 2018. “Urban Heat Island Analysis Using the Landsat 8 Satellite Data: A Case Study in Skopje, Macedonia.” Proceedings 2(358): 1-5. doi: 10.3390/ecrs-2-05171.

Karen C. Nelson and Palmer, Margaret A. 2007. “Stream temperature surges under urbanization and climate change: data, models, and responses.” Journal of the American Water Resources Association. 43(2): 440-452.

Kaushal, Sujay S, Gene E Likens, Norbert A Jaworski, Michael L Pace, Ashley M Sides, David Seekell, Kenneth T Belt, David H Secor, and Rebecca L Wingate. 2010. “Rising Stream and River Temperatures in the United States.” Frontiers in Ecology and the Environment 8 (9): 461-466. doi:10.1890/090037.

Lo, C. P., D. A. Quattrochi, and J. C. Luvall. 1997. “Application of high-resolution thermal infrared remote sensing and GIS to assess the urban heat island effect.” Int. J. Remote Sensing 18(2): 287-304. Doi: https://doi.org/10.1080/014311697219079.

Macarof, Paul and Florian Statescu. 2017. “Comparison of NDBI and NDVI as Indicators of Surface Urban Heat Island Effect in Landsat 8 Imagery: a Case Study of Iasi.” PESD 11(2): 141-150. doi: 10.1515/pesd-2017-0032.

Martin, Philippe, Yves Baudouin, Philippe Gachon. 2015. “An alternative method to characterize the Surface Urban Heat Island.” International Journal of Biometeorology 59:849–861.

Nelson, Kären C., and Margaret A. Palmer. 2007. “Stream Temperature Surges under Urbanization and Climate Change: Data, Models, and Responses.” Journal of the American Water Resources Association 43 (2): 440-452. doi: 10.1111/j.1752-1688.2007.00034.x

Noble, Richard D. and Alan P. Jackman. 1980. “Predicting the Natural Water Temperature Profile Throughout a River Basin.” J. Environmental Systems. 9(4): 361-381. doi: 10.2190/HYVQ-75JB-7GA6-7TYP

Pagliaro, Megan D., and Jason H. Knouft. 2020. “Differential effects of the urban heat island on thermal responses of freshwater fishes from unmanaged and managed systems.” Science of the Total Environment 723: 1-9. doi: 10.1016/j.scitotenv.2020.138084.

Paul, Michael J., and Judy L. Meyer. 2001. “Streams in the Urban Landscape.” Annual Review of Ecology and Systematics 32: 333-65. doi:10.1007/978-0-387-73412-5_12.

Rousta, Iman, Md Omar Sarif, Rajan Dev Gupta, Haraldur Olafsson, Manjula Ranagalage, Yuji Murayama, Hao Zhang, Terence Darlington Mushore. 2018. “Spatiotemporal analysis of land use/land cover and its effects on surface urban heat island using Landsat Data: A case study of metropolitan city Tehran (1988–2018).” Sustainability 10:1–25.

Sagris, Valentine, Mait Sepp. 2017. “Landsat-8 TIRS data for assessing urban heat island effect and its impact on human health.” IEEE Geoscience and Remote Sensing Letters 14:2385–2389.

Schweighofer, Julian A. V., Michael Wehrl, Sebastian Baumgärtel, Joachim Rohn. 2021. “Calculating Energy and Its Spatial Distribution for a Subsurface Urban Heat Island Using a GIS-Approach.” Geosciences. 11(24): 1-14. doi: 10.3390/geosciences11010024

Sechu GL, Nilsson B, Iversen BV, Greve MB, Børgesen CD, Greve MH. 2021. “A stepwise GIS approach for the delineation of river valley bottom within drainage basins using a cost

distance accumulation analysis." Water. 13:1–15.

Simwanda, Matamyo, Manjula Ranagalage, Ronald C. Estoque, Yuji Murayama. 2019. "Spatial analysis of surface urban heat islands in four rapidly growing African cities." Remote Sensing 11:1–20.

Tan, Jianguo, Youfei Zheng, Xu Tang, Changyi Guo, Liping Li, Guixiang Song, Xinrong Zhen, Dong Yuan, Adam J. Kalkstein, Furong Li, and Heng Chen. 2010. "The urban heat island and its impact on heat waves and human health in Shanghai." Int J Biometeorol 54: 75-84. doi: 10.1007/s00484-009-0256-x.

U.S. Geological Survey. 2022. "Landsat Collection 2 (C2) U.S. Analysis Ready Data (ARD) Data Format Control Book (DFCB)." Department of the Interior. 3.0.

Wang, Chuyuan, Soe W. Myint, Zihua Wang, Jiyun Song. 2016. "Spatio-Temporal Modeling of the Urban Heat Island in the Phoenix Metropolitan Area: Land Use Change Implications." Remote Sensing. 8(185): 1-17. doi: 10.3390/rs8030185

Wrzesiński, Dariusz and Renata Graf. 2022. "Temporal and spatial patterns of the river flow and water temperature relations in Poland." Journal of Hydrology and Hydromechanics. 12(1): 12-29. doi: 10.2478/johh-2021-0033

Yang, Xiaoshan, Yuan Chen, Lilliana L.H. Peng, Qingqing Wang. 2020." Quantitative methods for identifying meteorological conditions conducive to the development of Urban Heat Islands." Building and Environment 178:1–11.

Yow, Donald M. 2007. "Urban Heat Islands: Observations, Impacts, and Adaptation." Geography Compass 1227-1251. doi: 10.1111/j.1749-8198.2007.00063.x

Zhang et al. 2009. "Bi-temporal characterization of land surface temperature in relation to impervious surface area, NDVI and NDBI, using a sub-pixel image analysis." International Journal of Applied Earth Observation and Geoinformation. 11: 256-264.

Zhou, Bin, Diego Rybski, Jürgen P. Kropp. 2017. "The role of city size and urban form in the

Surface Urban Heat Island." Scientific Reports 7:1–9.

Zhou, Decheng, Jingfeng Xiao, Stefania Bonafoni, Christian Berger, Kaveh Deilami, Yuyu Zhou, Steve Frolking, Rui Yao, Zhi Qiao, and José Sobrino. 2019. "Satellite Remote Sensing of Surface Urban Heat Islands: Progress, Challenges, and Perspectives." Remote Sensing 11 (48): 1-36. doi:10.3390/rs11010048.